FAULT-CONTROLLED DOLOSTONE GEOMETRIES IN A TRANSGRESSIVE-REGRESSIVE SEQUENCE STRATIGRAPHIC FRAMEWORK

S. YAO[*,†], E. GOMEZ-RIVAS[‡,*], J.D. MARTÍN-MARTÍN[‡], D. GÓMEZ-GRAS[§], A. TRAVÉ[‡], A. GRIERA[§] and J. HOWELL[*]

[*] *Department of Geology and Geophysics, School of Geosciences, University of Aberdeen, King's College AB24 3UE Aberdeen, Scotland, UK (E-mail: yaoshuqing15@163.com)*
[†] *Geoscience Documentation Center, China Geological Survey, 100083 Beijing, China*
[‡] *Departament de Mineralogia, Petrologia i Geologia Aplicada, Universitat de Barcelona (UB), Martí i Franqués s/n, 08028 Barcelona, Spain*
[§] *Departament de Geologia, Univeristat Autònoma de Barcelona, 08193 Bellaterra, Spain*

ABSTRACT: *This study investigates the geometries of fault-controlled dolostone geobodies and their structural and sequence stratigraphic controls, which provide new insights for the prediction and production of fault-controlled dolomitized hydrocarbon reservoirs. A very thick succession (>1600 m) of Aptian-Albian shallow-marine carbonates of the Benassal Formation that crop out in the Benicàssim area (Maestrat Basin, eastern Spain) is partly replaced by dolomite, resulting in dolostone geometries ranging from massive patches to stratabound bodies. Detailed mapping, systematic logging and correlation were carried out to characterize the structural, sedimentary and sequence stratigraphic framework in the area and to constrain the principal controls on the full-range of dolostone geometries. The results show that carbonate sediments accumulated in a half graben stacked in three transgressive-regressive (T-R) sequences. Large-scale massive dolostone patches (with up to kilometre extension) form near large-scale faults indicating that they acted as entry points for warm dolomitizing fluids into the basin. These dolostone patches laterally pass to large stratabound bodies that extend for long distances (at least 7 km) away from feeding faults, forming a continuum. The presence of a regional unconformity and a clastic fine-grain low-permeability unit (Escucha Formation) on top of the Benassal Formation likely constrained the dolomitization fluids to an up to 580 m thick interval below the base of the Escucha Formation. Thus, only limestones within this interval, corresponding to the two uppermost T-R sequences, were dolomitized. There is a clear relationship between the stratigraphic framework and the preferred replaced beds. Dolomitization preferentially affected sediments deposited in inner to middle ramp settings with predominant wackestone to packstone textures. Such facies are laterally most abundant in the east of the study area (i.e. basinwards) and vertically in layers around the maximum flooding zone of the top sequence, which is preferentially affected by dolomitization.*

Keywords: Aptian-Albian, diagenesis, fault-controlled dolomitization, Maestrat Basin, outcrop analogue, stratigraphic sequence.

This manuscript is published in the journal *Sedimentology* (2020), DOI:10.1111/sed.12739. This is an author version of the article. For the final copy-edited version, please visit: https://onlinelibrary.wiley.com/doi/abs/10.1111/sed.12739

INTRODUCTION

Carbonate reservoirs are estimated to contain 60% of the world's remaining oil reserves (Roehl and Choquette, 2012). They typically exhibit a heterogeneous distribution of petrophysical properties, and consequently are challenging to explore, develop and produce. The main difficulties are associated with the fact that the distribution of porosity and permeability, and thus reservoir quality, in carbonate rocks is strongly affected by a variety of post-depositional diagenetic processes such as compaction, dissolution, cementation and mineral replacement (e.g. Tucker, 2009; James and Jones, 2015) that often occur at different times in the burial history resulting in a complex paragenetic evolution. The lateral and vertical extension of diagenetic products (cements, dissolution vugs, stylolites, etc.) are very difficult to characterize in three dimensions using subsurface data, especially since drill core only represents a very small fraction of the reservoir (e.g. Howell *et al*., 2014).

Dolomitization (i.e. the replacement of calcite with dolomite) is one of the most important diagenetic processes affecting limestone successions. It occurs in a wide range of environments and modifies the pore space geometry and volume as well as permeability (e.g. Allan and Wiggins, 1993; Warren, 2000; Machel, 2004). Dolomitization is a widely studied diagenetic process for understanding controls on fluid flow in carbonates (e.g. Whitaker *et al*., 2004; Qing and Mountjoy, 1992, 1994) because, unlike other diagenetic processes such as cementation or dissolution, the effects of dolomitization are easy to visualize on outcrops and drill core in many cases due to the colour and texture change associated with mineral change. Outcrop studies on dolomitization are thus essential for understanding how diagenesis impacts reservoir quality, and to unravel the key controls on diagenetic fluid flow producing rock alterations (e.g. Mansurbeg *et al*., 2016).

There are several types of dolomitization (for comprehensive reviews see Hardie, 1987; Warren, 2000; Machel, 2004; Whitaker *et al*., 2004), among which fault-controlled high-temperature dolomitization (HTD) is particularly relevant (see review by Davies and Smith, 2006) both from a scientific and economic point of view. High-temperature dolostone normally forms when warm fluids are transported up faults and invade the host limestones, resulting in the replacement of calcite with dolomite as well as in the formation of dolomite cement. The flow of high-temperature dolomitizing fluids in limestone successions can result in a variety of replacement geometries, from massive patches next to faults (e.g. Wilson *et al*., 2007; Sharp *et al*., 2010; Dewit *et al*., 2012), to stratabound geobodies that extend for long distances away from them (e.g. Sharp *et al*., 2010; Lapponi *et al*., 2011; Martín-Martín *et al*., 2013, 2017; Dewit *et al*., 2014; Gomez-Rivas *et al*., 2014; Gasparrini *et al*., 2017; Hollis *et al*., 2017).

The majority of published studies dealing with fault-controlled dolostones focus on the stratigraphic, petrographic and geochemical characterization of outcrop analogues, with the aim of providing an overall picture on how the dolomitization process is controlled by depositional facies, diagenesis and structures. Recent representative studies include the analysis of outcrops in the Zagros belt in Iran (e.g. Sharp *et al*., 2010; Lapponi *et al*., 2011), the Vasque-Cantabrian Basin in Spain (e.g. López-Horgue *et al*., 2010; Shah *et al*., 2010; Dewit *et al*., 2012; Dewit *et al*., 2014; Gasparrini *et al*., 2017), the Iberian Chain in Spain (e.g. Nadal, 2001; Martín-Martín *et al*., 2013, 2015, 2017; Corbella *et al*., 2014; Gomez-Rivas *et al*., 2014), the Oman mountains (e.g. Vandeginste *et al*., 2013;

Beckert *et al*., 2015), North America (e.g. Azmy *et al*., 2008; Diehl *et al*., 2010; Lavoie *et al*., 2010; Slater and Smith, 2012; Morrow, 2014; and see review by Davies and Smith, 2006; and references therein), the Alps (Ronchi *et al*., 2012; Jacquemyn *et al*., 2015), the Apulia Carbonate Platform (Rustichelli *et al*., 2017) and the Suez Rift (Hollis *et al*., 2017), among many others. These studies highlight a series of aspects that impact fault-controlled dolomitization, including the characteristics of fault zones that act as entry points for dolomitization fluids, the permeability and composition of host limestones (associated with depositional facies and pre-dolomitization diagenesis), and the properties of fracture networks that can facilitate or prevent dolomitization by acting as either conduits or barriers for dolomitization fluid flow.

Despite the recent advances on the understanding of high-temperature dolomitization, there are still fundamental open questions on how this process operates and controls the volume, geometry and distribution of the resulting diagenetic geobodies. Key questions to be addressed include: (i) what is the spatial relationship between faults and dolostone geobodies at multiple scales; (ii) which, if any, sedimentary facies and stratigraphic sequences are preferentially replaced; (iii) to what extent do pre-dolomitization diagenetic products control replacement; and (iv) what is the role of low-permeability sedimentary units as seals for dolomitizing fluids?

These questions were tackled through the study of the high-temperature dolostones of the Benicàssim outcrop analogue (Maestrat Basin, eastern Spain), with the overarching aim of providing an improved framework for the prediction of high-temperature dolomitization geometries in shallow-marine carbonates. In this area, a very thick pile (>1600 m) of Lower Cretaceous shallow-marine carbonates of the Benassal Formation are well-exposed. The limestones are partially dolomitized in close association with regional faults. The Benicàssim area has been the focus of several recent studies (e.g. Martín-Martín *et al*., 2013, 2015, 2017; Corbella *et al*., 2014; Gomez-Rivas *et al*., 2014), which focused on dolostones with stratabound distribution, and dealt with the analysis of depositional facies, diagenetic evolution and source of the dolomitization fluids. These studies did not tackle controls on variable dolomitization geometries across different fault blocks and in relation to the sedimentary facies and stratigraphic sequences.

GEOLOGICAL SETTING

Structure, transgressive-regressive sequences and lithofacies

The Benicàssim area is located in the south-eastern part of the Maestrat Basin (eastern Spain) (Fig. 1). This rift basin developed during the Late Jurassic-Early Cretaceous syn-rift cycle of the intraplate Iberian Rift System (Salas and Casas, 1993; Salas *et al*., 2001). The Maestrat Basin was subsequently inverted during the late Eocene-early Oligocene Alpine Orogeny (Guimerà *et al*., 2004), and then experienced extension during the late Oligocene-Miocene to form the present-day western margin of the Valencia Trough (Roca and Guimerà, 1992).

The study area is characterized by two systems of extensional faults that intersect each other: (i) the NNE-SSW striking and south-east-dipping Benicàssim Fault system; and (ii) the east-west striking and south-dipping Campello and Juvellús Fault system (Martín-Martín et al., 2013) (Fig. 1). According to the latter authors, the Benicàssim and Campello faults are inherited from the Hercynian Orogeny and were reactivated as extensional

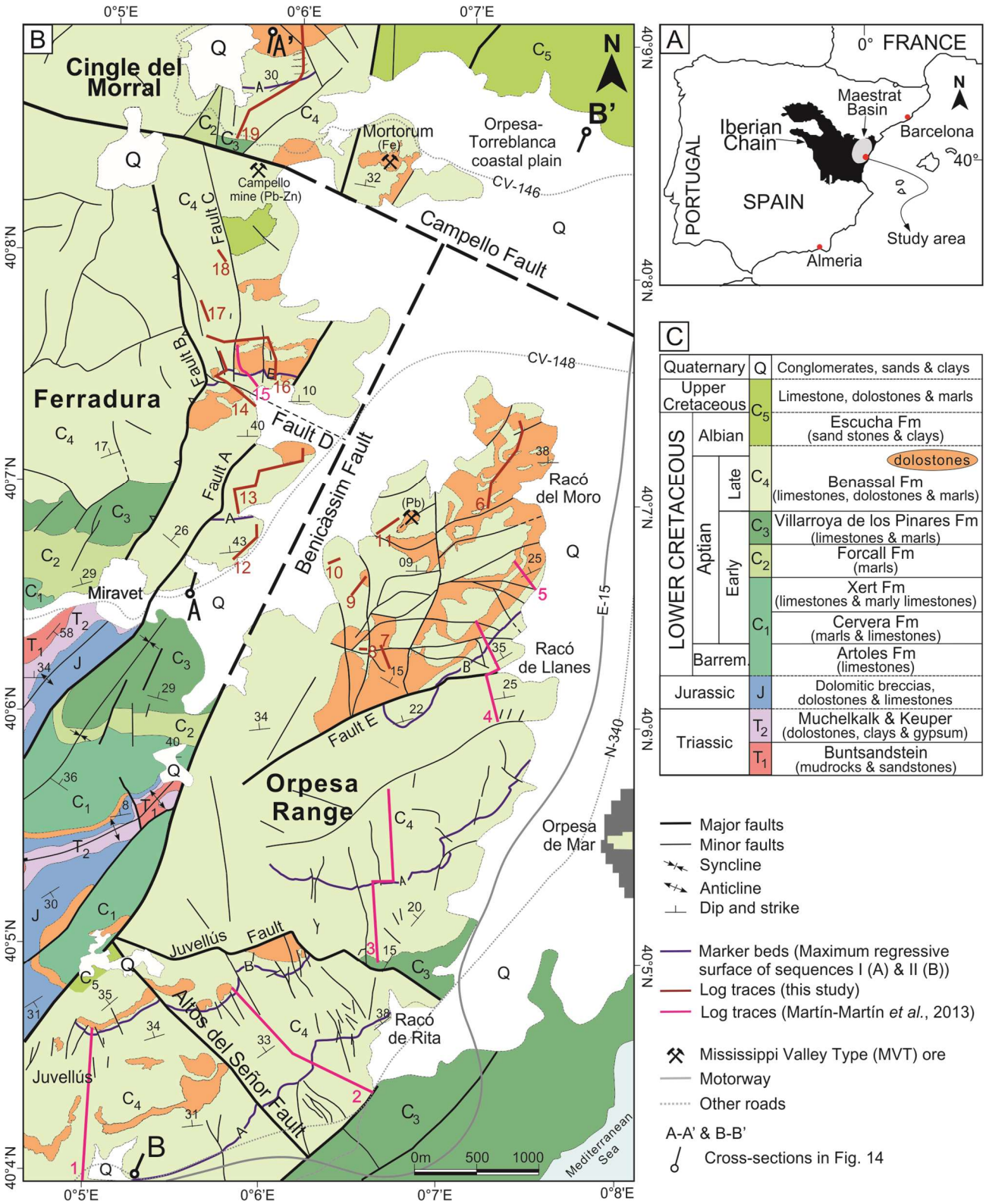

Quaternary	Q	Conglomerates, sands & clays
Upper Cretaceous	C_5	Limestone, dolostones & marls
LOWER CRETACEOUS – Albian	C_5	Escucha Fm (sand stones & clays)
LOWER CRETACEOUS – Aptian Late	C_4	dolostones; Benassal Fm (limestones, dolostones & marls)
LOWER CRETACEOUS – Aptian Early	C_3	Villarroya de los Pinares Fm (limestones & marls)
LOWER CRETACEOUS – Aptian Early	C_2	Forcall Fm (marls)
LOWER CRETACEOUS – Aptian Early	C_1	Xert Fm (limestones & marly limestones)
LOWER CRETACEOUS – Aptian Early	C_1	Cervera Fm (marls & limestones)
LOWER CRETACEOUS – Barrem.	C_1	Artoles Fm (limestones)
Jurassic	J	Dolomitic breccias, dolostones & limestones
Triassic	T_2	Muchelkalk & Keuper (dolostones, clays & gypsum)
Triassic	T_1	Buntsandstein (mudrocks & sandstones)

Fig. 1. (A) Simplified map of the Iberian Peninsula showing the location of the Maestrat Basin. (B) Geological map of the Benicàssim area showing the distribution of dolostones and their relationship with large-scale faults (modified from Martín-Martín *et al.*, 2013). The traces of stratigraphic logs used in this study are indicated with pink solid lines (logs reported here for the first time) and red solid lines (logs previously reported in the literature). (C) Chronostratigraphic chart showing the lithogical units cropping out in the study area. T (Triassic), J (Jurassic) and C (Cretaceous) in the legend represent cartographic units.

Table 1. Summary of the key characteristics of lithofacies types (LFT). LFT1 to LFT12 are taken from Martín-Martín *et al*. (2013) with slight modifications based on new data from the Ferradura and Cingle del Morral fault blocks. LFT13 to LFT15 are newly defined lithofacies.

Lithofacies type (LFT)		Characteristic components	Sedimentary features	Depositional environment
1	Green marl	Echinoids, brachiopods (Rhynchonellida and Terebratulida) and bivalves	Marls with green, gray or ocher color, nodular bedding, laminar siltstones, metric to tens of meters bedding	Outer ramp
2	Cross-bedded peloidal and orbitolinid packstone to grainstone	Peloids, orbitolinids, echinoids, miliolids	Tabular bedding, high to low-angle cross-stratification, sharp bases (occasionally), decimetric to metric bedding	Inner to outer ramp
3	Peloidal grainstone	Peloids	Massive bedding, bioturbation, sharp bases (occasionally), decimetric to metric bedding	Inner to middle ramp
4	Orbitolinid wackestone to rudstone and marl	Orbitolinids	Massive to wavy bedding, centimetric to metric bedding	Inner to outer ramp
5	Coral sheetstone	Sheet-like corals	Slightly marly bedding, decimetric to metric bedding	Inner to middle ramp
6	Coral limestone	Platy, tabular and domal corals in live position. Coral fragments	Tabular massive to nodular bedding, lithophagid borings, metric bedding	Inner to middle ramp
7	Rudist floatstone to rudstone	Requieniid and elevator rudists	Tabular massive to slightly nodular bedding, metric bedding	Inner to middle ramp
8	Grainstone with siliciclastic influence	Echinoids, peloids, intraclasts	Cross-bedding, tidal bundles, herring-bone stratification, metric bedding	Inner ramp
9	Spicule wackestone	Sponge spicules, undifferentiated shell debris	Massive to wavy bedding, bioturbation, silica nodules (occasionally), metric bedding	Outer ramp
10	Grainstone with hummocky cross-stratification	Peloids, orbitolinids	Cross-bedding, hummocky cross-stratification, bioclastic lags, graded beds, centimetric to decimetric bedding	Middle ramp
11	Bioclastic wackestone to packstone	Bivalves, other molluscs, sessile foraminifera, miliolids	Massive to wavy bedding, bioturbation, decimetric to metric bedding	Inner to outer ramp
12	Ooid grainstone	Ooids	Cross-bedding, centimetric to decimetric bedding	Inner to middle ramp
13	Foraminifera & green algae wackestone to grainstone	Miliolids, orbitolinids, Dasycladales green algae, aggregate grains	Cross-lamination (occasionally), decimetric to metric bedding	Inner to middle ramp
14	Echinoid-sponge-rich packstone to rudstone	Echinoid, sponge, bivalves, braquiopoda, belemnites, corals	Cross-lamination (occasionally), with intercalations of grey marls, metric bedding	Middle to outer ramp
15	Corals embedded in marls	Corals, sponges, echinoids	Domal, platy and tabular coral colonies in life position deposited in grey to ocher marls, metric to tens of meters bedding	Middle ramp

faults during the Mesozoic. During the Late Jurassic and Early Cretaceous rifting more than 2 km of syn-rift deposits were accommodated in the Benicàssim area. A significant proportion of these sediments constitute the Late Aptian-Early Albian Benassal Formation, which represents a limestone succession dominated by shallow-marine carbonates with a present-day thickness of more than 1600 m (Martín-Martín et al., 2013).

The Benassal Formation was deposited on a carbonate ramp very rich in orbitolinids, rudists, corals and algae with scarce siliciclastic input (Tomás *et al*., 2008; Martín-Martín *et al*., 2013). Based on the analysis of the sedimentary succession cropping out in the Orpesa Range fault block (see Fig. 1), the latter authors defined twelve lithofacies types (LFT; Table 1) and three transgressive-regressive (T-R) sequences (Fig. 2). The transgressive systems tract (TST) of sequence I is characterized by basinal marls, whereas the regressive systems tract (RST) is marked by peloidal and orbitolinid grainstones, and peloidal and coral facies. The latter deposits are topped by a thick unit of rudist floatstones that represent the most regressive deposits of sequence I. The latter unit shows an erosional surface with palaeokarst at its top, revealing subaerial exposure (sequence boundary A in Fig. 1). The TST of sequence II initiates with a few metres of sandy limestones displaying tidal bundles and cross-bedding. Above, most of the TST is characterized by orbitolinid-rich and spicule-rich muddy facies. The RST of sequence II is distinguished by coral-bearing and rudist-bearing limestones stacked in a progressive

pattern, that alternate with hummocky cross-stratified grainstones and peloidal grainstones. The RST ends with a several tens of metres thick unit made up of rudist and *Chondrodonta* bivalves with floatstone to boundstone textures, the top of which represent the maximum regressive surface (MRS) of the T-R sequence II. The TST of sequence III is mainly formed by nodular bedded bioclastic limestones containing mud-drapes and orbitolinids that are overlain by up to a hundred metres of dolostones with several limestone stringers dominantly composed of mud-dominated facies. One of these stringers corresponds to spicule-rich wackestones at the top of which the maximum flooding zone (MFZ) is placed. The bottom of the RST is partially dolomitized and passes upwards to ooidal-rich, bioclastic-rich and peloidal-rich facies. The top of sequence III is faulted and covered, and thus the boundary with the Escucha Formation was not recognized in the Orpesa Range. Within the Maestrat Basin the top of Benassal Formation is bounded by a regional subaerial unconformity represented by a palaeokarst that is overlaid by up to 90 m of fine-grained tidal claystones and sandstones of the Escucha Formation (Salas *et al*., 2001).

Fault-controlled dolostones

The Benassal Formation is partly dolomitized throughout the Benicàssim area. This replacement, as well as locally associated galena-sphalerite (Pb-Zn) Mississippi Valley Type (MVT) ore deposits, are closely related to the aforementioned Campello and Benicàssim fault systems (Martín-Martín et al., 2013, 2015, 2017; Gomez-Rivas et al., 2014). These authors studied massive and stratabound dolostone bodies that extend up to 7 km away from basement faults, with individual maximum thicknesses of up to 150 m.

Field and analytical data provided by Martín-Martín *et al*. (2015) from an analysis of the Orpesa fault block (Fig. 1) indicate that the dolomitization of the Benassal Formation host limestones took place after a major stage of mechanical and chemical compaction, and thus during burial. The latter authors described four types of dolomite: (i) most of the replacive mass is formed by planar-s to non-planar dolomite crystals with characteristic cloudy appearance and mimetic fabric (Fig. 3A to C); (ii) mimetic dolomite appears frequently recrystallized in close association with fractures and permeable areas, forming planar-s to non-planar replacive dolomite crystals with cloudy cores and clear rims (Fig. 3D); (iii) planar-e crystals that formed after precipitation of clear dolomite rim overgrowths over replacive cores (i.e. overdolomitization) (Fig. 3E); and (iv) saddle dolomite filling fractures, stylolitic and vuggy porosity (Fig. 3F). The dolomitization took place during with the regional Late Cretaceous thermal event (average age of ±89 Ma), a time that is considered the most probable age of replacement (Martín-Martín *et al*., 2017). According to Martín-Martín *et al*. (2015), dolomitization took place at burial depths of less than 1.2 km for the stratigraphically lower dolostones and significantly less burial (about 300 m) for the uppermost ones. The studies by Martín-Martín *et al*. (2015) and Martín-Martín *et al*. (2017) reveal that the petrographic and geochemical characteristics of massive and stratabound dolostone geobodies are very similar, both types of dolostones likely formed at the same time.

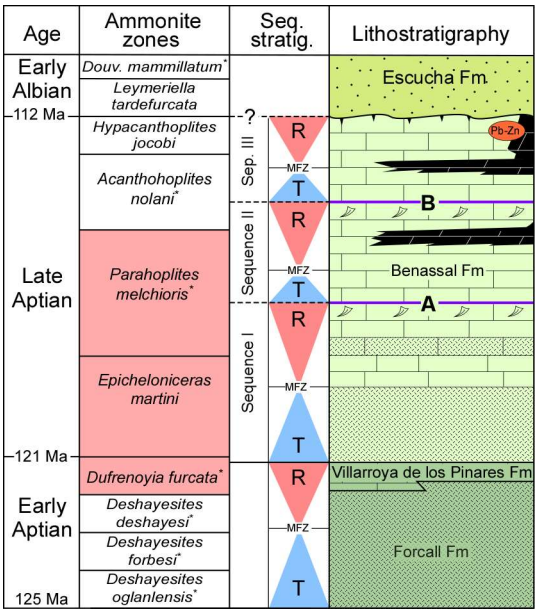

Fig. 2. Chronostratigraphy, biostratigraphy and lithostratigraphy chart showing the sequence stratigraphy framework of the Benassal Formation in the study area as well as the location of dolostones (black colour) (modified from Martin-Martín *et al.,* 2015). Ammonite biozones identified in the study area are shaded in red. Dashed lines in transgressive-regressive (T-R) sequences indicate lack of absolute dating, and purple lines denote the maximum regressive surfaces (MRS) of sequences I (A) and II (B) (see blue lines Fig. 1 for their trace on the geological map). MFZ, maximum flooding zone; R, regressive system tract (R); T, transgressive system tract (T). Bottom and top boundaries of lithological formations after Bover-Arnal *et al*., 2016.

The dolomitization fluids are interpreted as hydrothermal because their estimated temperatures (exceeding 80ºC and at least up to 110º) are considerably higher than host rock temperatures according to the geothermal gradient. These would have ranged between *ca* 30 and 60ºC from the uppermost to the lowermost replaced limestones, respectively (Gomez-Rivas *et al*., 2014). This study also revealed that the dolomitization fluids were likely derived from infiltrated seawater that exchanged with basin and basement rocks, resulting in up to 23% eq. wt. NaCl salinity. Geochemical and mass-balance calculations suggest that interstitial fluids alone could not account for the volume of dolomite, and that only a pervasive fluid circulation mechanism based on thermal convection could have provided a sufficient volume of fluids to produce the replacement reaction during the Late Cretaceous (Gomez-Rivas *et al*., 2014). Two-dimensional (2D) fluid flow and reactive transport simulations presented in Gomez-Rivas *et al*. (2010) and Corbella *et al*. (2014) suggest that the fluid flow system that produced the large-scale stratabound dolostone geobodies in this area probably had a strong lateral component and lasted for about a million years. There is no evidence from field and petrographic observations that the fluid that caused replacive dolomitization circulated at high pressure.

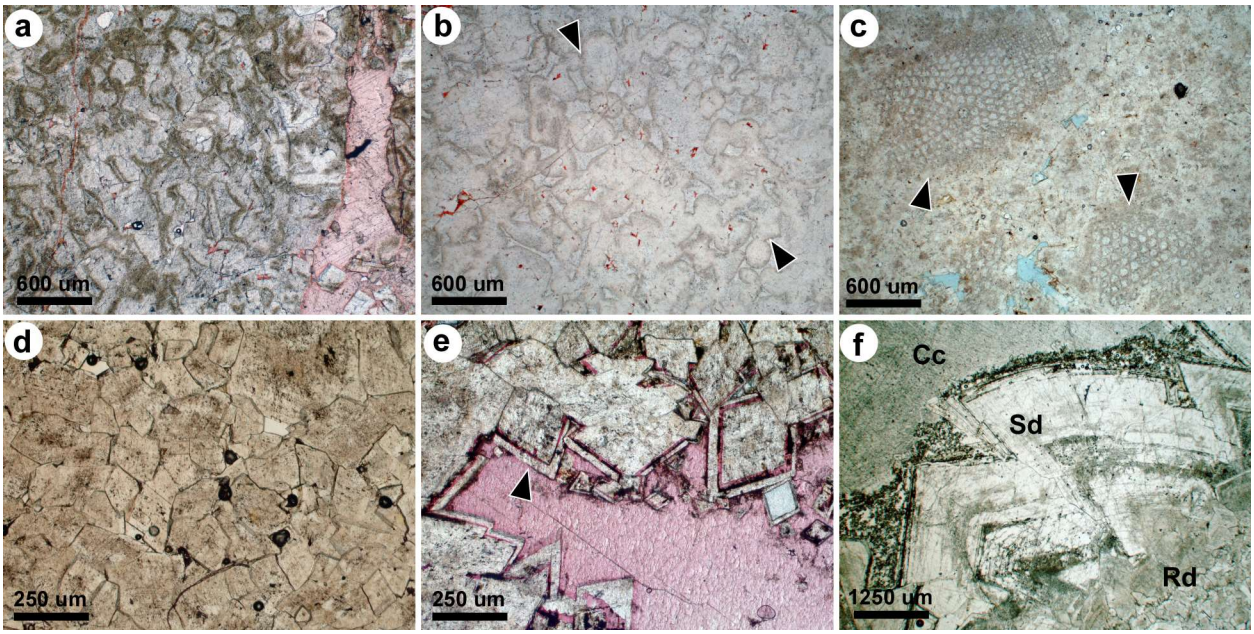

Fig. 3. Photomicrographs of dolomite textures. (A) Replacive dolomite crystal mosaic showing planar-s to non-planar textures and mimetic fabric (modified from Martín-Martín *et al.*, 2015). Plane polarized light. (B) and (C) Diffused light images of replacive dolomite crystal mosaic showing ghosts of peloids and orbitolinids (arrowed), respectively (modified from Martín-Martín *et al*., 2013). Note concavo-convex contacts (arrowed) between peloids in B, indicating dolomitization after some compaction (D) Replacive dolomite crystal mosaic showing planar-s to non-planar textures (modified from Martín-Martín *et al.*, 2017). Plane polarized light. (E) Replacive dolomite crystal mosaic showing dolomite cement (arrowed) in the form of rim overgrowth (modified from Martín-Martín *et al.*, 2015). Plane polarized light. (F) Large crystal of saddle dolomite (Sd) predating replacive dolomite crystal mosaic (Rd) and postdating late calcite cement (Cc) (modified from Martín-Martín *et al.*, 2013). Plane polarized light. Calcite in (A), (B) and (F) appears red after staining with Alizarin Red-S.

METHODS

Field mapping and logging were used to constrain: (i) the depositional lithofacies of the Benassal Formation and their distribution; and (ii) the distribution of dolostones and their association with faults, lithofacies and stratigraphic sequences (Figs 1, 4 to 7). The vertical and lateral distribution of lithofacies was based on 19 logs (with a total logged thickness of about 6000 m) that cover the three major faulted blocks of the study area (Orpesa Range, Ferradura and Cingle del Morral). Thirteen of these logs are reported here for first time (logs 6 to 14, and 16 to 19) and complement those published by Martín-Martín *et al*. (2013, 2017) in the Orpesa Range (logs 1 to 5) and Ferradura (log 15) blocks, respectively (Figs 4 to 7). Correlation between logs and faulted blocks was based on photo panels, key surfaces, bedding traces and characteristic facies. The correlation is partially calibrated by ammonite specimens (see Martín-Martín *et al*., 2013 and Garcia *et al*., 2014). The datum for the stratigraphic correlation between faulted blocks is placed at the base of the Escucha Formation following Salas *et al.* (2001).

Fifty rock samples including limestones and dolostones were collected during field work for thin section description to determine rock textures and components, and thus for depositional lithofacies classification. The classification of limestone textures follows Dunham (1962) and Embry and Klovan (1971). A total of 15 lithofacies were considered including those defined by Martín-Martín *et al*. (2013) (LFT 1 to 12) and three additional types defined in this study (LFT 13 to 15) (see summary in Table 1; Figs 8 and 9).

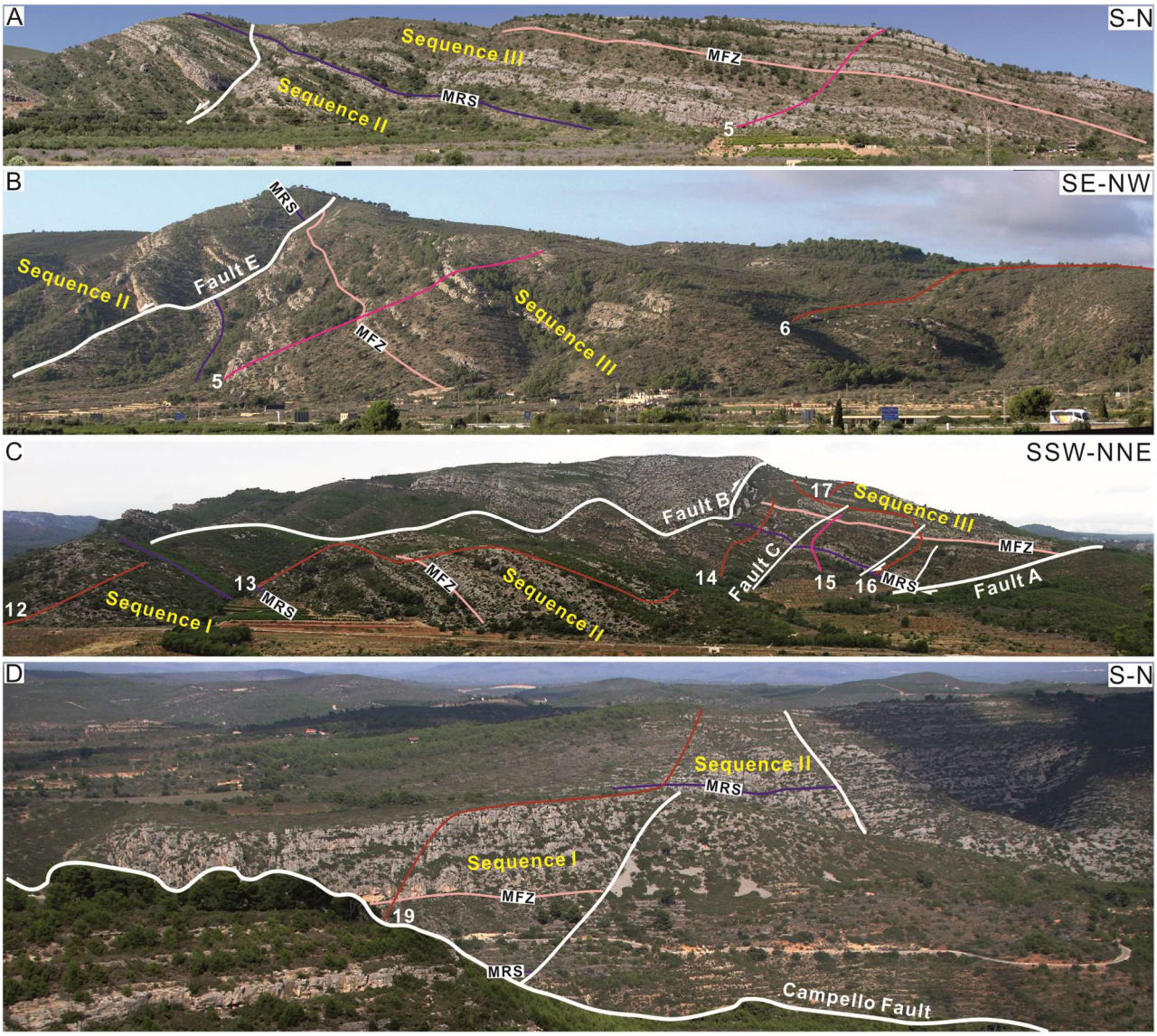

Fig. 4. Panoramic views of the Benassal Formation in (A-B) the north of the Orpesa Range (view is ~4 km wide), (C) the Ferradura (view is ~2 km wide) and (D) the Cingle del Morral (view is ~1.3 km). The traces of field logs are indicated with dark red lines. Sequence stratigraphy surfaces of the Benassal Formationm are maximum regressive surface (MRS) and maximum flooding zones (MFZ). Grey rocks correspond to host limestones, while dolostones present a brownish colour. Numbers in A, B, C and D indicate the corresponding log in Fig. 1, 5, 6, 7 and 12.

The Benassal Formation is arranged into three T-R sequences following the sequence stratigraphy framework defined in the study area by Martín-Martín *et al*. (2013) and, on a wider scale, in the Maestrat Basin by Bover-Arnal *et al*. (2009, 2016). Accordingly, the T-R sequences interpreted from new logs presented here are based on the lithofacies evolution and their stacking pattern in deepening to shallowing trends, or *vice versa* (see Catuneanu *et al*., 2009). Due to difficulty in precisely locating the maximum flooding surface (MFS) within each sequence, a maximum flooding zone (MFZ) *sensu* Strasser *et al*. (1999) was defined in this study.

The geometries of dolostones are recognized based on their dimensions and spatial association with faults and bedding. The areal extent of the dolostone bodies was assessed using conventional field mapping and virtual outcrop models (VOs). Dolostone bodies of eleven selected locations were ground checked with emphasis on the transition between

different geometries, and their potential relationship with depositional facies, T-R sequences, fault systems, fractures and stylolites. LiDAR (Light Detection and Ranging) and an UAV (unmanned aerial vehicle) were used to collect geospatially constrained field data in order to build high-resolution VOs of three selected outcrops (e.g. Buckley *et al*., 2008, 2010, 2013). The LiDAR model was a RIEGL VZ-2000 with a Nikon D100 camera, and the UAV was a DJI Phantom 3 Advanced. Five local high-resolution models were used to compare in detail dolostone geobodies geometries in different outcrops.

RESULTS

Sequence stratigraphy and lithofacies evolution

The characteristics of lithofacies evolution and sequence stratigraphy framework vary across the three study fault blocks (Orpesa Range, Ferradura and Cingle del Morral). Accordingly, they are summarized for each fault block below (see Table 1 and Fig. 2).

Orpesa Range

The Orpesa Range represents the hanging wall block of both the Campello and Benicàssim faults (Figs 1, 4 and 5). The newly reported log in this fault block (log 6) is 231 m long and represents the uppermost part of T-R sequence III of the Benassal Formation reported in the area by Martín-Martín *et al*. (2013). Taking into account the stratigraphic data reported by these authors, the maximum thickness of the Benassal Formation cropping out in this fault block is up to 1606 m (Fig. 5).

The new section (log 6) appears faulted at its bottom and comprises 185 m of dolostones replacing both mud-dominated and grain-dominated facies. Accordingly, limestone stringers within dolostones, which range in thickness between 10 to 30 m, are composed of bioclastic wackestones (LFT11), rudist floatstones (LFT7), coral limestones (LFT6) and peloidal grainstones (LFT3). The top of the section is covered by Quaternary deposits, and thus the boundary with the Escucha Formation is not exposed in the area. Based on field observations, however, the covered succession is assumed to be in the range of several tens to a few hundred metres (Fig. 5).

Ferradura

The Ferradura area represents the footwall block of the Benicàssim Fault and the hangingwall block of the Campello Fault (Figs 1 and 6). The thickness of the Benassal Formation measured in this area is 1215 m (logs 12 to 18), although the total thickness is assumed to be one to several hundred metres higher as the bottom and top of the Benassal Formation are covered by vegetation and Quaternary deposits (Fig. 6).

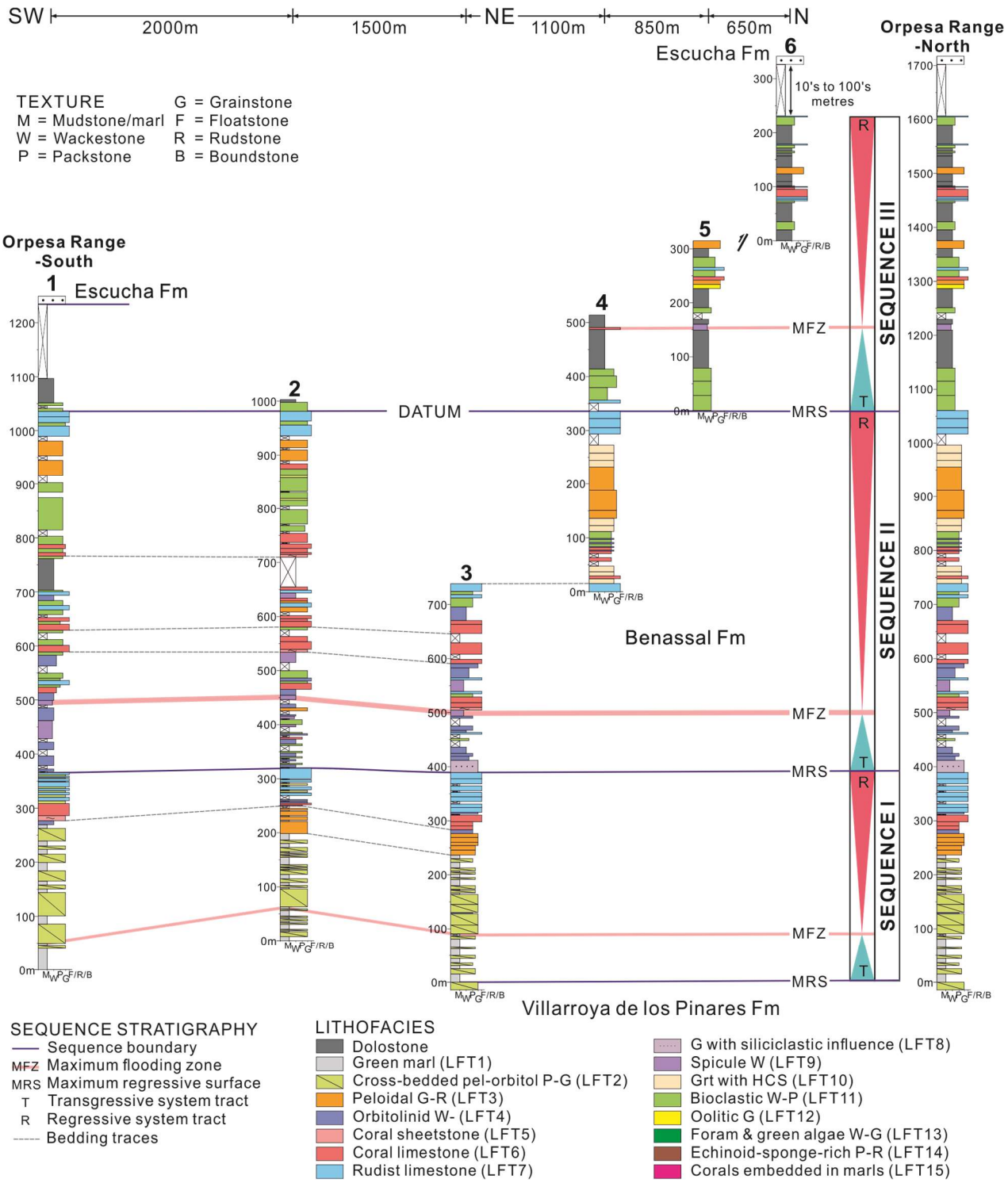

Fig. 5. Correlation of six partial stratigraphic logs of the Benassal Formation along the Orpesa Range showing the facies distribution and T-R sequences. Logs 1 to 5 are redrawn after Martín-Martín *et al.* (2013). The Orpesa Range-North represent a composite section based on logs 2, 3, 4, 5 and 6. Textural classification in this and subsequent figures *sensu* Embry and Klovan (1971). See Figs. 1 and 4 for log location. Pel (peloidal), Orbitol (orbitolinid), HCS (hummocky cross-stratification) and Foram (foraminifer).

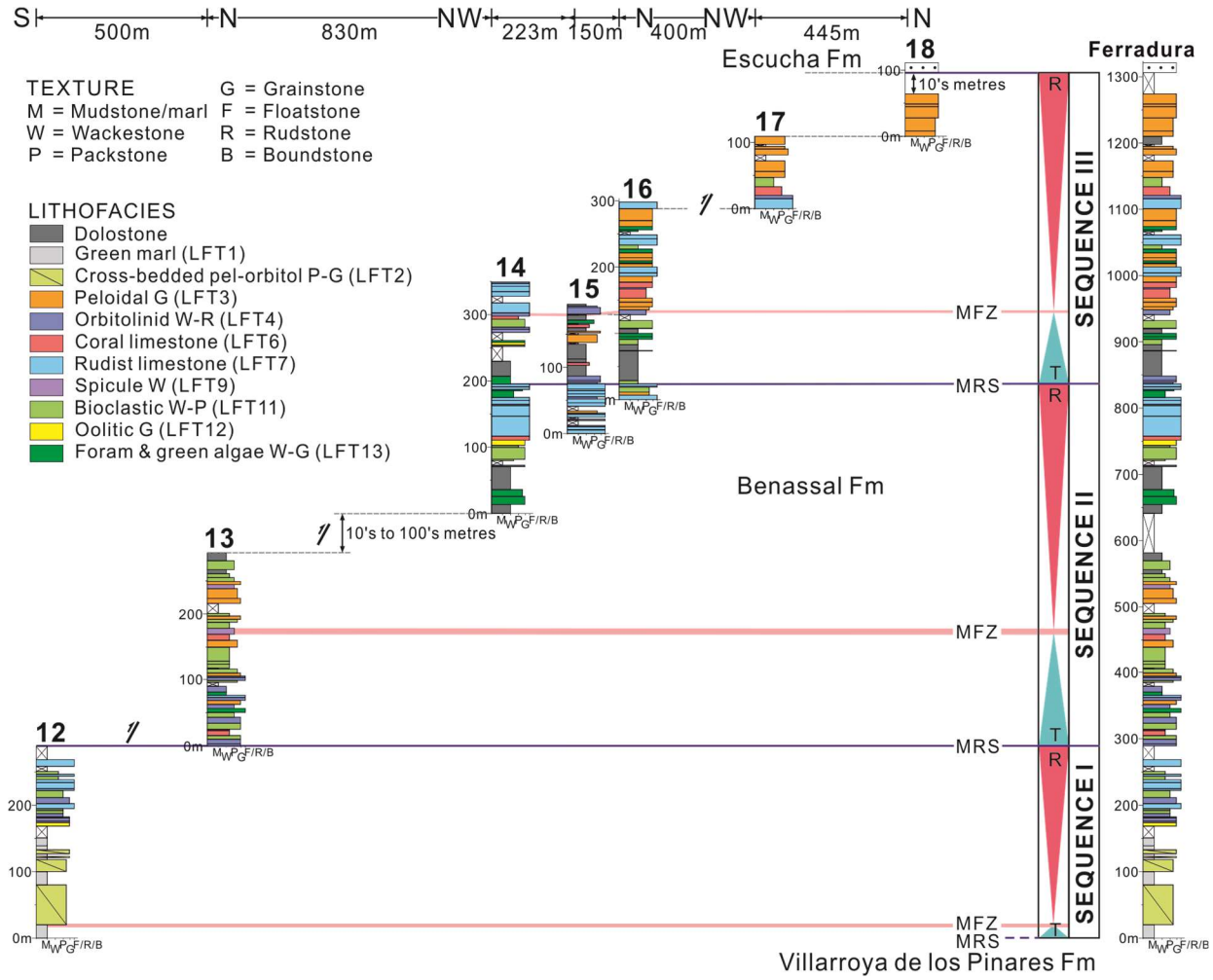

Fig. 6. Correlation of seven partial stratigraphic logs of the Benassal Formation along the Ferradura, showing the facies distribution (See Figs 1 and 4 for log location). Log 15 is redrawn after Martín-Martín *et al*. (2017). The Ferradura section is a composite section based on logs 12 to 18. Pel (peloidal), Orbitol (orbitolinid), HCS (hummocky cross-stratification) and Foram (foraminifer). See Fig. 5 for sequence stratigraphy legend.

T-R sequence I is 289 m thick and is well exposed along the road CV-148 (log 12; Figs 1 and 4C). The TST is characterized by ochre-coloured marls with echinoids and terebratulida brachiopods (LFT1) with several metre-thick intercalations of peloidal and orbitolinid grainstones (LFT2) rich in glauconite and quartz grains together with minor mica (Figs 6, 8A and B). The MFZ of sequence I is placed at the top of the first and thickest marly unit. Above, the RST is topped by a thick bed-set of rudist floatstones (LFT7) containing minor nerineid gastropods. The rudist appear mostly fragmented, locally forming bouquets in life position, and are dominated by requieniids (*Toucasia sp.*). The rudist floatstones, which are covered and faulted towards the top, are the most regressive deposits of sequence I, and thus the MRS and the boundary between sequences I and II is placed at the top (Figs 4 and 6).

T-R sequence II is about 548 m thick (log 13 and 14; Figs 4C and 6). The TST is characterized by the predominance of mud-dominated facies dominated by orbitolinid-rich facies (LFT4) that pass upwards to several tens of metre-thick bed-sets of bioclastic wackestones to packstones (LFT11). Intercalated between the latter facies appears a bed-set composed of very fine-grained packstones with sponge spicules, calcispheres and chert nodules (LFT9) (Fig. 8C). The MFZ is placed at the top of the spicule-rich facies,

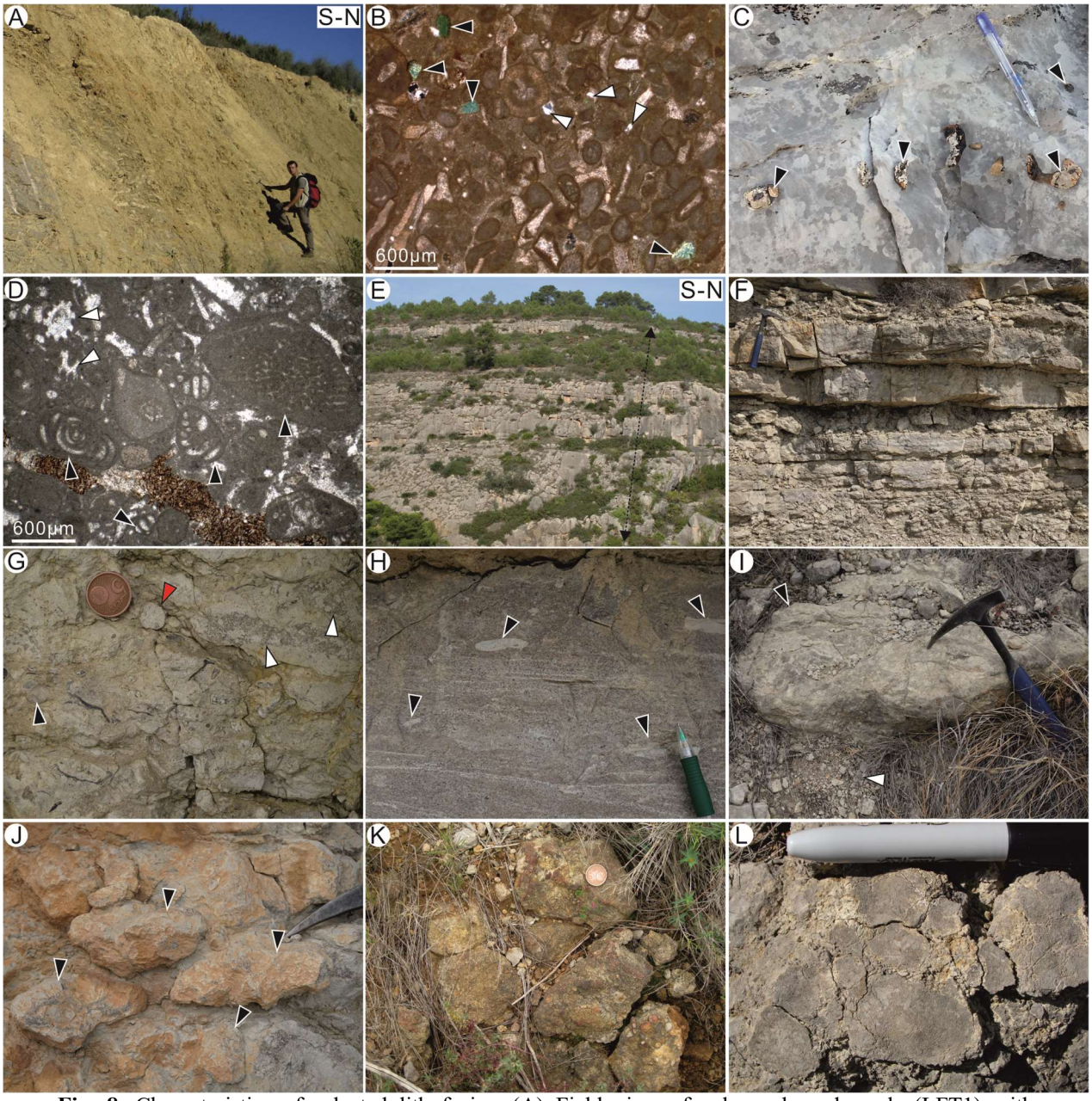

Fig. 8. Characteristics of selected lithofacies. (A) Field view of ochre-coloured marls (LFT1) with intercalated peloidal and orbitolinid grainstones (LFT2). The person for scale is 1.85 m high. (B) Photomicrograph of LFT2 showing abundant glauconite (black arrows) and quartz grains (white arrows). Plane polarized light. (C) Field view of very fine-grained packstones with abundant chert nodules (black arrows) typical of LFT9. Thin section analysis indicates that this lithofacies is rich in sponge spicules and calcispheres. The pen is 13.5 cm long. (D) Photomicrograph of LFT 13 showing the association of foraminifers (black arrows) and dasycladals green algae. Plane polarized light. (E) Field view of a peloidal grainstones (LFT3) unit from log 18 (the arrow represents ~70 m approximately). (F) Field view of LFT14 showing a coarsening and thickening up cycle made of echinoid-sponge-rich packstones to grainstones. The hammer is 32 cm long. (G) Close view of LFT14 showing the poorly sorted character and the presence of echinoids (black arrow), corals (white arrows) and sponges (red arrows). The coin is 2.1 cm in diameter. (H) Close view of LFT14 showing cross-lamination, mud pebbles (black arrows) and mud drapes. The pen is 4 cm long. (I) Field view of LFT15 showing a coral colony in life position (black arrow) embedded in grey marls (white arrow). The hammer is 32 cm long. (J) Field view of LFT15 showing centimetre-sized coral colonies (black arrows) touching each other. The hammer is 7 cm long. (K) Field view of a conglomerate made of centimetre-sized quartz grains (LFT8). The coin is 1.6 cm in diameter. (L) Close view of mud cracks appearing at the top of surface of cycles. The pen is 10 cm long.

which are interpreted as the deepest water deposits of sequence II. Above, the lower part of the RST comprises peloidal (LFT3), bioclastic (LFT 11) and a several tens of metres-thick unit of foraminifera and green algae packstone and grainstone (LFT13) facies that appear dolomitized and covered by Quaternary deposits (Figs 6 and 8C). The RST of sequence II ends with an *ca* 80 m thick unit of massive and several metre-thick beds of rudist and *Chondrodonta* floatstone to boundstones (LFT7). The rudist bivalves are dominated by large requieniids (*Toucasia sp.)* and radiolitids specimens. The MRS of sequence I is placed at the top of this rudist bed set (Fig. 6).

Sequence III, which is 469 m thick, starts with a TST that shows a 115 m thick unit of dolostones replacing mud-dominated and grain-dominated facies as indicated by several stringers made up of coral, bioclastic and peloidal limestones (logs 14 to 16; Figs 4C and 6). The dolostones are topped by orbitolinid rudstones (LFT4) with abundant chert nodules, which are considered the most transgressive deposits and at the top of which is placed the MFZ. Above, the RST is dominated by a set of several metre-thick beds made of medium to coarse-sized peloidal grainstones (LFT3) (Logs 16 to 18; Figs 4C and 8E). The top of the T-R sequence III, and thus the top boundary of the Benassal Formation, is covered, and not recognized in the Ferradura fault block. However, the presence in the surroundings of loose and fragmented beds of ochre-coloured and quartz-rich sandstones typical of the Escucha Formation suggests that the boundary between both formations is nearby (Fig. 1).

Cingle del Morral

The Cingle del Morral is located at the footwall block of the Campello Fault and the Benassal Formation is only 674 m thick here (log 19; Figs 1 and 7). This thickness represents 456 m measured in outcrops and 234 m more of cover calculated assuming a constant bed dip until the top boundary with the Escucha Formation is reached (Figs 4D and 7). The bottom boundary of the Benassal Formation with the underlying Villarroya de los Pinares Formation is characterized by a sharp lithological change from well-bedded and cross-laminated ooidal grainstones below to marly facies (Figs. 7).

Sequence I, which is 232 m thick, shows a TST dominated by marly packstones to rudstones rich in coarse-sized skeletal components, echinoderms and coral fragments (LFT14) that gradually pass to ochre-coloured marls with echinoids, terebratulids brachiopods and belemnites (LFT1) (Figs 7, 8F to H). These transgressive marls include the ammonite species *Epicheloniceras sp.* and *Caseyella sp.* indicating a Late Aptian age. The MFZ is placed at the top of the marly unit, which represents the most transgressive deposit of sequence I. Above the marls, the TST is characterized by a *ca* 20 m thick set of centimetre to decimetre limestone beds exhibiting poorly sorted packstone to rudstone textures rich in echinoids and sponges (LFT14). The latter limestones show erosive bases, cross-bedding, and thin intercalations of grey marls, and form coarsening and thickening up cycles. Together with the echinoderms and sponges, these limestones are abundant in mud pebbles and mud drapes, terebratulid and rhynchonellid brachiopods, corals, oysters, pectinids, gastropods, belemnites, ammonites and other unidentified components. These limestones pass progressively upwards to grey marls containing coral colonies in life position, sponges and echinoids (LFT15), facies equivalent to those described in detail by Bover-Arnal *et al*. (2012) (Fig. 8I to J). The coral colonies, which reach up to one metre in height, are domal and tabular shaped and appear as individuals or growing one on top of the other. The corals show abundant *lithophaga* bivalve borings and their tops

frequently are the substrate for sponges, oysters and other undifferentiated organisms. Towards the top of this unit the corals considerably increase in abundance with respect to the marls forming patches of several metres (i.e. bioherms) between them (Fig. 8J).

The RST ends with a 20 m thick bed set of bioclastic wackestone to packstones with abundant coral fragments (LFT11) topped by 8 m of rudist limestones exhibiting floatstone to boundstone textures (LFT7). The rudist bivalves are dominated by large requieniids (*Toucasia sp.*) and radiolitid specimens, occasionally forming bouquets in life position. Together with rudists, *Chondrodonta* bivalves are locally abundant, forming the main skeletal component of the limestones. The latter floatstones, which represent the most regressive sediments of sequence I, show an erosive surface at their top where the MRS is placed (Fig. 6).

Sequence II and II are not defined, as the upper part of the succession is mostly covered. The sequence I however, is overlain by a 20 cm thick conglomerate made of cm-sized quartz pebbles that represents the sole evidence of siliciclastic sediments in the Cingle del Morral section (Fig. 8J). This siliciclastic deposit is considered time-equivalent to those of LFT8 that overly sequence I in the Orpesa Range (log 3; Fig. 4). The rest of the succession is characterized by miliolid and orbitolinid packstones with abundant green algae and aggregate grains (LFT13), and bioclastic (LFT11) and peloidal (LFT3) facies. The latter are laterally dolomitized at the outcrop scale, forming thin dolostone beds between the host limestones. Following the dolostones, the succession is characterized by several bed-sets of limestones with coral fragments and, less frequently, in life position (LFT6) that pass upwards to rudist floatstone (LFT7). These bed-sets are rich in ferruginized grains and are locally capped by mud cracks (Fig. 8L). The uppermost part of the outcropping section is mostly replaced by dolostones that show intercalation of limestones stringers made up of peloidal (LFT3) and rudist (LFT7) facies. The top of the section, and thus the top of the Benassal Formation, is covered although the overlaying Escucha Formation crops out further to the north. There, the Escucha Formation is made up of cross-laminated quartz-rich sandstones and grey marls.

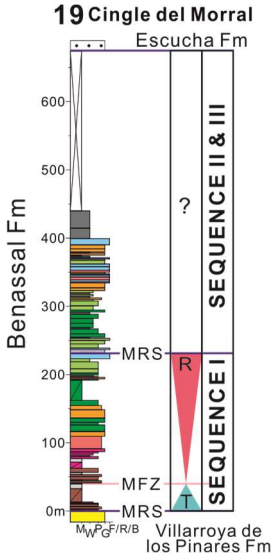

Fig. 7. Cingle del Morral section (log 19) showing the facies distribution in the footwall of the Campello Fault. See Figs 1 and 4 for log location. See Fig, 5 for lithofacies, texture and sequence stratigraphy legend.

Dolostone geometry and distribution

Dolostones extensively replace limestones of the Benassal Formation across the Benicàssim half-graben and are especially abundant in the hanging wall blocks of the Benicàssim and Campello faults, particularly south of their intersection (Fig. 1). Two main types of dolostone geobodies are distinguished in the Benicàssim area based on their dimensions and spatial association with faults and bedding (Table 2): (i) fault-controlled massive dolostone patches (Figs 9E to F, 10); and (ii) stratabound dolostones (Figs 10 and 11). Both types are described below.

1 Patches of massive, non-stratabound dolostones crop out close to faults at various scales, from metre-scale (Fig. 9E and F) to km-scale faults (Fig. 10A). In such cases dolomitization fronts cross-cut bedding. The massive dolostone patches have widths ranging from 300 to 1600 m and thicknesses varying between 20 to at least 200 m. Patches of massive dolostone with a pipe-like shape (*sensu* Sharp *et al*., 2010) follow fault traces upwards and appear rooted in stratabound dolostone bodies.

2 Stratabound dolostones are defined as dolostone bodies replacing specific beds (Figs 10A and 11). They are typically kilometres wide and are a few metres to hundreds of metres thick. Massive patches are typically connected with stratabound dolostone geobodies away from the feeding faults, in a continuous way so that the stratabound bodies are terminations of the massive ones (Fig. 10A).

The two main types of dolostone geobodies described here are continuous and present the same petrographic characteristics and diagenetic evolution (see Martín-Martín *et al*., 2015, 2017).

Table 2. Dolostone body dimensions and their characteristics

Location	HTD body			Width	Thickness	Feeding fault	Sequence
	Massive	Stratabound	Pipe	(km)	(km)		
Racó del Moro	1			1.4-1.6	>0.200		S3-RST
		1		>4	0.150	Campello	S3-MFS
		2		>2.2	0.020		S3-MFS
		3		>2	0.045		S3-RST
			1	0.02	0.100	Sub-seismic fault	S3-RST
Juvellús	2			0.3	0.180	Altos del Señor,	S2-RST
		4		>1.7	0.700	Benicàssim	S2-RST
		5		>1.5	0.050		S3-MFS
Ferradura	3			<0.8	0.020		S3-RST
		6		>2	>0.080	Campello	S2-RST
		7		>2	0.115		S3-MFS
Cingle del Morral		8		>1.1	0.002	Campello	S2-MFS
		9		>1.1	0.040		S2-RST

Dolostones are laterally continuous along the Orpesa Range fault block, from north to south. The largest massive patch in the area, which is spatially associated with the Campello Fault and appears in its hanging wall, is at least 200 m thick and 1400 to 1600 m wide and contains a few limestone stringers (Figs 1, 10A and B). This large patch passes laterally to large stratabound dolostone geobodies that act as its termination. The largest stratabound body has a maximum thickness of 150 m and extends for more than 7 km away from the Campello Fault, replacing host rocks of the upper part of the Benassal Formation (Figs 1, 10A and 12). Also in the Orpesa Range fault block, but away from the

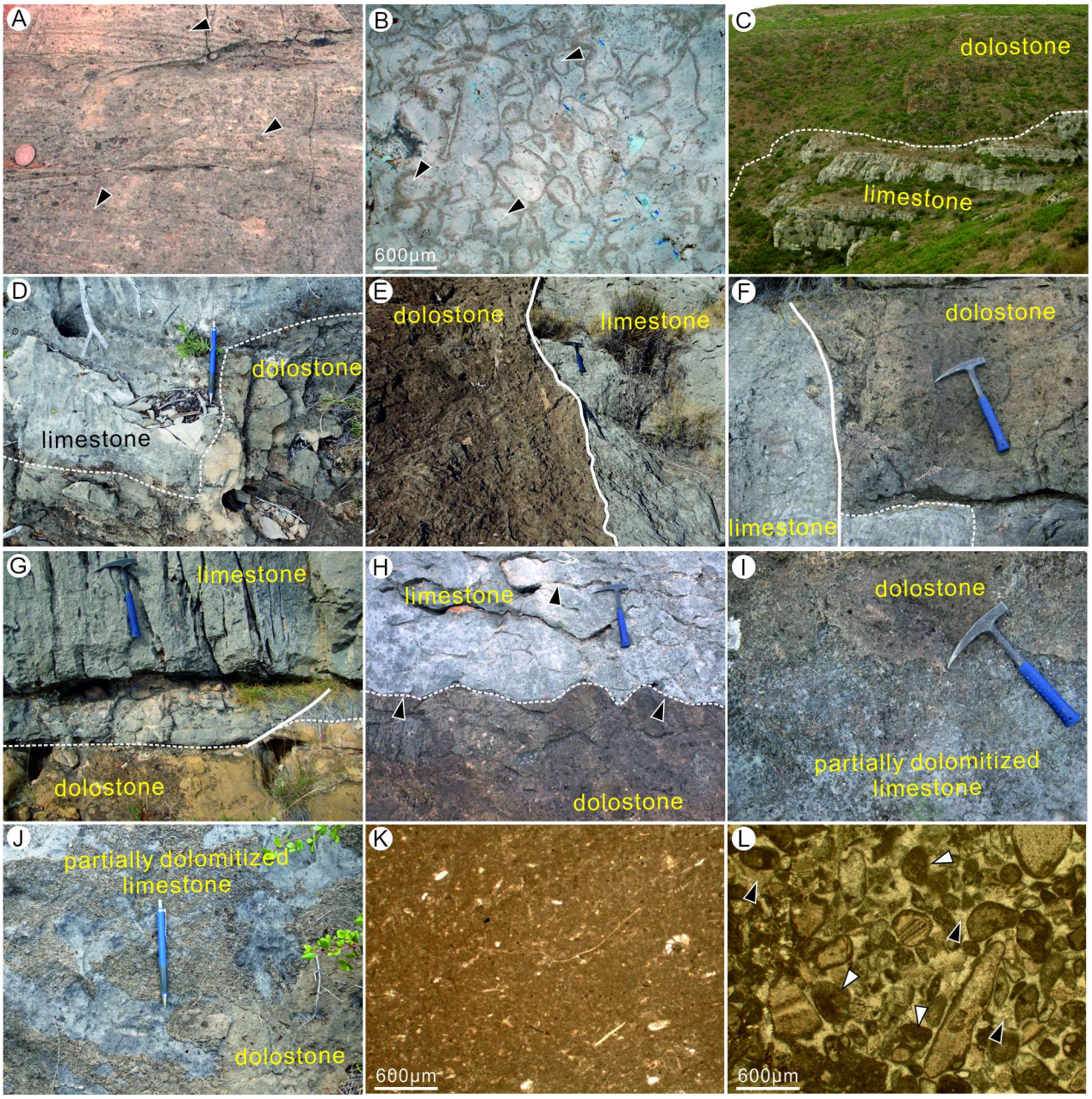

Fig. 9. Major characteristics of limestones and dolostones. (A) Close view of a dolostone, most probably dolograinstone, showing well-preserved cross-lamination (black arrows). The coin is 2.1 cm in diameter. (B) Photomicrograph of a replacive dolomite crystal mosaic showing ghosts of the original grain components, which are dominated by peloids (black arrows). Diffused light. (C) and (D) Field view of large (C) and small-scale (D) dolomitization fronts (dashed lines) that are laterally pinching out. View in (C) is about 180 m high. The pen in (D) is 13.5 cm long. (E) and (F) Close-up view of sharp dolomitization fronts (dashed line) corresponding to an outcrop-scale fault and a fracture (white line), respectively. The hammer is 32 cm long. (G) and (H) Close-up views of sharp dolomitization fronts (dashed line) mainly along bedding planes and wavy stylolites (black arrows), respectively. The hammer is 32 cm long. (I) and (J) Close-up views of transitional (i.e. not sharp) dolomitization fronts, showing partially replaced limestones. Note that most of the replaced limestones corresponds to skeletal components. The hammer in (I) is 32 cm long. The pen in (J) is 13.5 cm long. (K) Photomicrograph of sponge spicule wackestone (LFT9). Plane polarized light. (L) peloidal (white arrows) grainstone (LFT3) completely cemented by calcite (black arrows). Plane polarized light.

Campello Fault, some kilometre long faults with a similar strike (e.g., the Altos del Señor Fault and Fault D, which strike NW-SE to WNW-ESE) are surrounded by massive dolostone patches (hundreds of metres wide and tens of metres thick) (Fig. 1). A *ca* 500

m wide massive dolostone patch cropping out in the hanging wall of the Altos del Señor Fault passes laterally to a stratabound dolostone geobody that is 70 m thick and at least 1700 m long (Fig. 5). Stratigraphically, these beds represent the lowermost dolostones in the whole study area. The equivalent beds are not replaced in the north part of the Orpesa Range fault block (i.e. close to the Campello Fault). The bottom boundary of this body is about 550 m below the base of the Escucha Formation (Figs 1, 10A and 12). The stratigraphically uppermost dolostones lie just about 130 m below the base of the Escucha Formation in this fault block. Dolostones in the Orpesa Range fault block replace sediments of T-R sequences II and, in a larger extent, sequence III (Fig. 5). In the north, where the depocentre is located, only the T-R sequence III is dolomitized affected by replacement, with a slightly preference for sediments deposited in the RST. However, in the southern part of this fault block, the replacement affects sediments of the sequence III and the RST of sequence II.

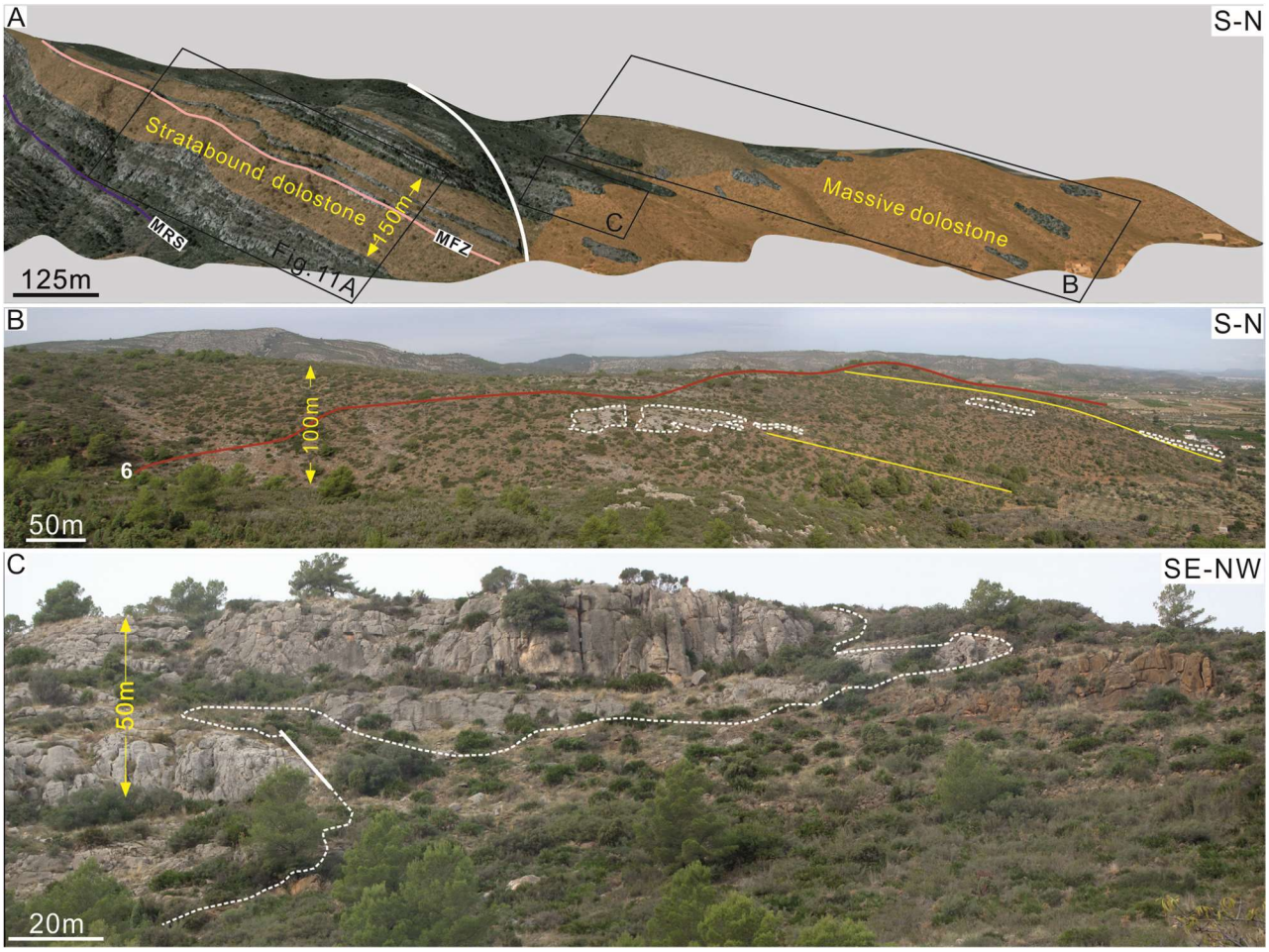

Fig. 10. (A) Google Earth view of a dolostone geobody in the north part of the Orpesa Range, forming a continuum that include massive dolostone patches (dark orange) passing to stratabound dolostones (light orange) towards the south. The feeder Campello Fault is about 1400 to 1600 m away from the transition zone towards the north. (B) Field view of massive dolostone patch showing several non-replaced limestone stringers (dashed lines). The red line corresponds to the trace of log 6. Yellow lines indicate bedding planes. (C) Field view of the transition zone from massive dolostone patch to stratabound dolostones. The dolomitization front (dashed line) is laterally bounded by outcrop-scale faults (white solid line).

Dolostones in the Ferradura fault block replace limestones of various depths corresponding to the middle and upper parts of the Benassal Formation (Figs 1, 6 and 12). The lowermost dolostones in this area crop out about 2200 m away from the Campello

Fault and replace limestones at a depth ranging from 750 to 600 m below the top of the Benassal Formation. These sediments correspond to the regressive part of sequence II. The lower part of these dolostones is formed by a few thin dolomitized beds with individual thicknesses of a few metres. They are in contact with spicule wackestones to packstones (LFT9) that contain silica nodules (Fig. 8B). The upper part of these dolostones is affected by several faults and presents a thickness of about 80 m. Limestone stringers within these dolostone bodies correspond to foraminifera and green algae grainstones (LFT13) with abundant orbitolinids and miliolids (Fig. 6). Dolostones replacing the upper part of the Ferradura block are dominated by a thick stratabound dolostone body (115 m thick, 550 m long) that terminates at a fault and contains abundant limestone stringers (Figs 6 and 11B). This lies about 1500 m south of the Campello Fault and corresponds to the transgressive part of sequence III. A small massive dolostone patch (20 m thick) located about 800 m away from the Campello Fault appears stratigraphically higher than the aforementioned stratabound geobody (see patch close logs 17 and 18 in Figs 1 and 6). This thin massive dolostone patch passes laterally to highly-cemented peloidal grainstone (LFT3) and belongs to the regressive part of sequence III. Limestones cropping out below the base of the Escucha Formation are formed by LFT3 and are only partly dolomitized here. All the uppermost dolostone bodies in this fault block are bounded at their west side by Fault C, which is a NNW-SSE trending normal fault with a length of 1800 m and an offset of tens of metres. The corresponding beds of these dolostones are not replaced in the footwall block of Fault C except for a small patch (log 14; Figs 6 and 11B). Dolostones in the Ferradura fault block are restricted to a vertical interval whose bottom and top are about 750 m and 70 m below the base of the Escucha Formation (Figs 8E and 12).

Dolostones in the Cingle del Morral fault block replace limestones of the middle part of the Benassal Formation and present a stratabound geometry, extending at least 1000 m away from the Campello fault. They are restricted to a vertical interval ranging from 100 to 400 m below the base of the Escucha Formation (Fig. 12). Dolostones replace several thin limestone beds (decimetre to 3 m thick) of foraminifera and green algae wackestones to grainstones (LFT13) in the lower part of the body, and a relatively thicker unit (50 m) above (Figs 7 and 8L). These dolostones correspond to sequence II.

Dolostones commonly preserve depositional characteristics of the host limestones, including bedding and lamination (Fig. 9A). The replaced skeletal components (e.g., orbitolina, echinoid plates, miliolids, rudist fragments and other bioclasts) can be distinguished in the weathered surface of dolostones as well as in thin section (Fig. 9B). These mimetic textures (Fig 9C to F) reveal that several lithofacies were dolomitized, including peloidal grainstones (LFT3), orbitolinid wackestones to rudstones (LFT4), coral limestones (LFT5), rudist floatstones (LFT7), spicule wackestones (LFT8) and bioclastic wackestones to packstones (LFT11). Dolostone bodies show unreplaced limestone stringers usually composed of muddy facies with suture and sharp peak and wave-like stylolites (*sensu* Koehn *et al*., 2016; Fig. 9H and K) or grainy facies that are strongly cemented with calcite that precipitated prior to dolomitization (for details of the paragenetic evolution see Martín-Martín *et al*., 2015, 2017) (Fig. 9L). The stringers can be up to 10 m thick and extend for a few hundreds of metres (Figs 10B and 11B).

Dolomitization fronts

Dolomitization fronts are mostly sharp (Fig. 9C to H) but they very occasionally are marked by a transition zone, ranging from 0.5 to 1 m, of pure limestone to pure dolostone (Fig. 9I and J). Dolostone bodies are observed to pinch out at various scales, from tens of metres to centimetres (Fig. 9C and D). However, most dolomitization fronts are laterally bounded by faults at a range of scales, from major faults with lengths of hundreds of metres to outcrop-scale faults and fractures with lengths of metres (Fig. 9E to G). Vertically, many dolomitization fronts correspond to bedding planes or bed-parallel stylolites (Fig. 9G and H). Vertical dolomitization fronts can be composed of a combination of faults, fractures and stylolites in certain cases (Fig. 9C, D, F and G).

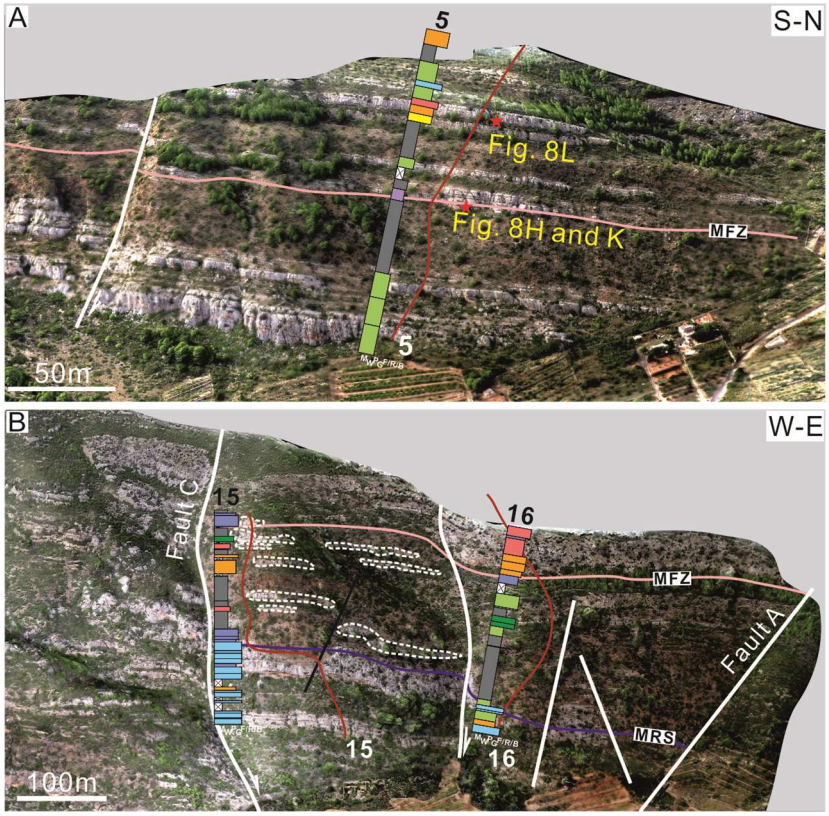

Fig. 11. Photographic view of stratabound dolostones taken from UAV virtual outcrop models in the north of the Orpesa Range (A) and the Ferradura (B) respectively. Note that stratabound dolostones are significantly more abundant (thicker and with longer extension) and with less limestone stringers in the Orpesa Range when compared with the Ferradura. The outlines of selected limestone stringers within dolostone bodies are indicated with white dash lines in (B). The units represented in the superimposed logs represent those beds found laterally next to the log. See Fig. figure 5 for lithofacies, texture and sequence stratigraphy legend. Faults are noted by white lines.

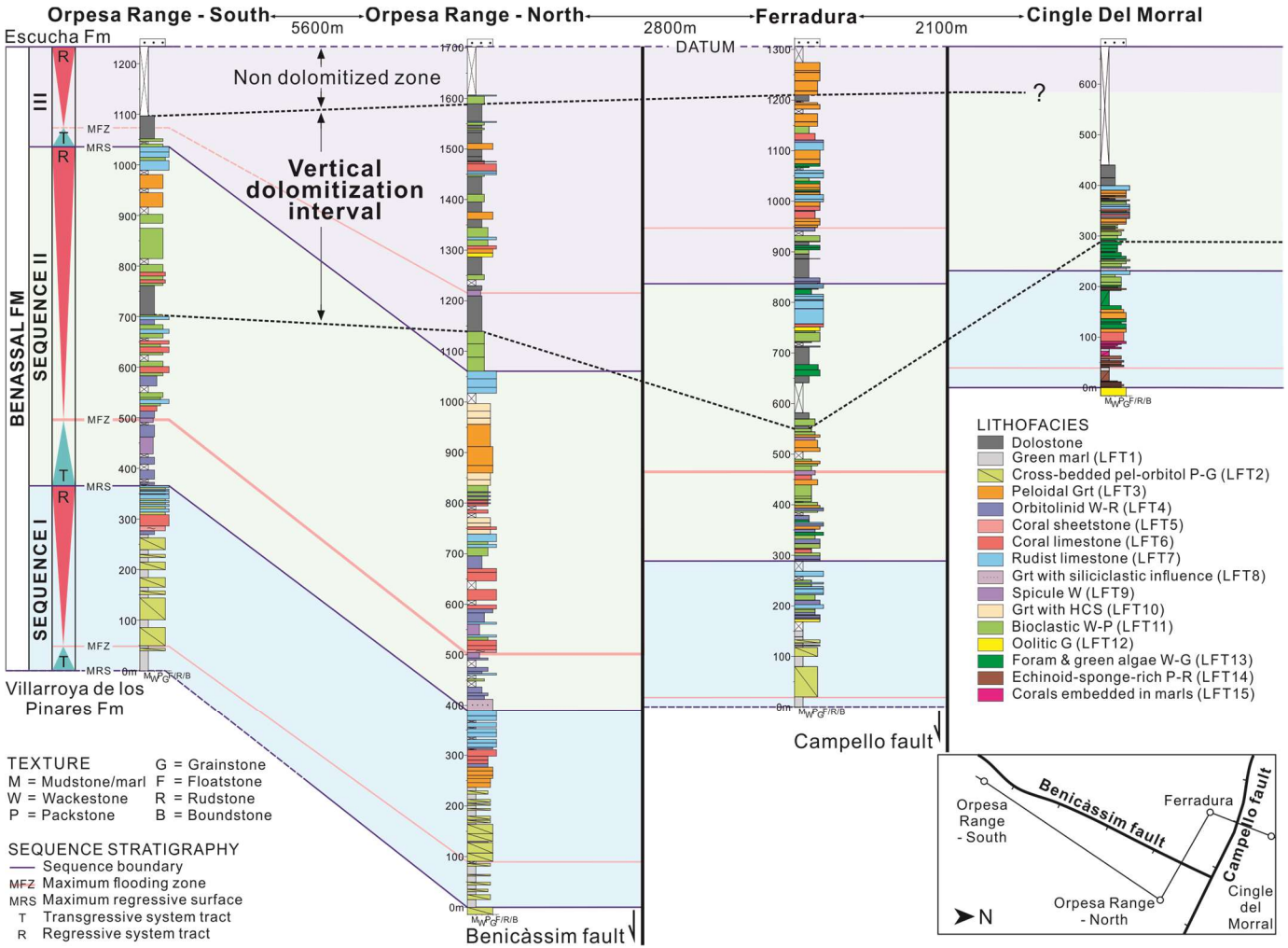

Fig. 12. Correlation of the Benassal Formation across the three fault blocks showing the distribution of dolostones in the stratigraphic framework. The sequences are coloured in blue (Sequence I), green (Sequence II) and purple (Sequence III). The grey coloured zone refers to the vertical dolomitization interval, which represents the lowest and highest occurrences of dolostones within the Benassal Formation. Note that the datum corresponds to the base of the Escucha Formation (top of the Benassal Formation) to highlight the effect of faulting during deposition. Pel (peloidal), Orbitol (orbitolinid), HCS (hummocky cross-stratification) and Foram (foraminifer).

DISCUSSION

Structure of the Benicàssim half-graben

Correlation of sedimentary logs of the exposed Benassal Formation in the Benicàssim area reveals significant variations in sediment thickness across the three main blocks defined by the Campello and Benicàssim major faults (Figs 5, 6, 7, 12 and 13). The most important structure at the time of deposition was the W-E trending Campello Fault, as indicated by the >1600 m thick succession observed in its hanging wall (Orpesa Range block) compared to 700 m at its footwall (Cingle del Morral block) (Figs 7 and 13). This N-S structural framework is consistent with a half-graben basin with a depocentre immediately south of the Campello Fault. Along the hanging wall of the Campello Fault, the Benassal Formation progressively thins from <1600 m in the north to ~1250 m in the south, likely resulting in a regional onlap in that direction (Figs 5 and 12).

The east-to-west structure of the study area was influenced by the N-S trending Benicàssim Fault that records a difference of 300 m in the thickness of the Benassal Formation between the hanging wall (Orpesa Range block) and the footwall (Ferradura block) (Figs 6 and 13). The variation in thickness between faulted blocks confirms that the Benicàssim Fault was also active during the deposition of the Benassal Formation. This east-to-west framework indicates that the carbonate platform was tilted towards the east, and thus the basin depocentre was located in the north-east of the study area.

The analysis of the Benassal Formation lithofacies and their stacking pattern throughout the study area reflects a dominant shallow-marine carbonate platform with very scarce terrigenous influx that evolved from basinal to inner platform environments with time (Figs 12 and 13). The depositional system was interpreted by Martín-Martín *et al*. (2013) as a ramp-type carbonate platform based on: (i) the excellent lateral continuity of facies belts, which indicates a carbonate ramp with a minimum width in the range of kilometres; (ii) a very similar stacking patterns of lithofacies across fault blocks; and (iii) the lack of step-like structures.

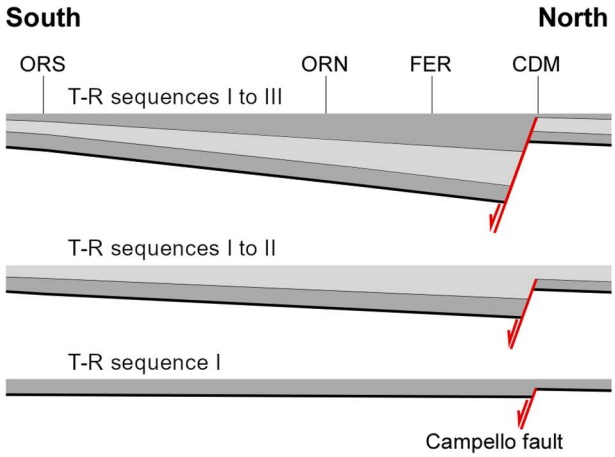

Fig. 13. Sketch of the south to north structure present in the study area illustrating the association of the Campello fault (red line) withthe variation in thickness of Sequence 1 to 3. ORS (Orpesa Range-South section), ORN (Orpesa Range-North section), FER (Ferradura section), CDM (Cingle del Morral section), T-R (Transgressive-Regressive).

Controls on the geometries of dolostone geobodies

The Benicàssim half-graben hosts a series of large-scale dolostone geobodies that constitute an excellent example of well-exposed massive diagenetic alteration. These dolostone bodies crop out in an area that is at least 3.2 km long and 9.0 km wide (Fig. 1). The arrangement, petrographic and geochemical characteristics suggest that these dolostones are high-temperature and closely related to the Campello and Benicàssim faults and were therefore interpreted as fault-controlled (see geological setting; Gomez-Rivas *et al*., 2014; Martín-Martín *et al*., 2015, 2017).

Two types of dolostone geometries have been recognized, showing a clear spatial association between them: (i) fault-controlled massive patches, including dolostone pipes; and (ii) stratabound dolostones. Field data suggest that fault-controlled massive dolostone patches laterally evolve to stratabound bodies, forming a continuum equivalent to the classical Christmas tree pattern at multiple scales (Fig. 10A), but with a very long, lateral stratabound component. Dolostone pipes are rooted in the thickest stratabound dolostones and are spatially relatively close to the massive patches. Such association of geometries are common in most cases of fault-controlled dolomitization and are typically interpreted as being genetically related to the same dolomitization process (e.g. Davies and Smith, 2006; Wilson *et al*., 2007; Sharp *et al*., 2010; Lapponi *et al*., 2011). However, there are also cases in which such geometries have been formed during different events (Hollis *et al.*, 2017). In either case, the relative extension of fault-controlled massive patches is a key factor for hydrocarbon exploration because good reservoir quality can typically be found close to the transition zone from massive patches to stratabound dolostones (e.g. Wilson *et al*., 2007).

Structural controls on replacement

Different faults in the study area are interpreted to have acted as feeders or barriers for dolomitization fluids at various scales. Based on results from this and previous studies, faults spatially associated with massive dolostone patches and dolostone pipes are interpreted to have acted as entry points for dolomitization fluids into the basin, in agreement with previous studies of fault-controlled dolomitization (e.g. Davies and Smith, 2006; Wilson *et al*., 2007; Sharp *et al*., 2010; Lapponi *et al*., 2011; among many others). Feeding faults in the study area are some of the syn-rift structures, chiefly the Campello Fault and a series of large-scale faults with a similar strike (such as the Altos del Señor Fault and Fault D) (see Fig. 1). According to field, petrographic and geochemical data from the area, these faults were likely connected in a way that the dolomitizing fluid came from underlying basin and basement rock units and then was distributed by these structures. Despite the different detachment level of the two dominant faults systems (Antolín-Tomás *et al*., 2007), the intersections of both systems very likely allowed their connectivity to allow fluid circulation. Moreover, geochemical and mass balance calculations (Gomez-Rivas *et al*., 2014), together with reactive transport models (Corbella *et al*., 2014) indicate that a pervasive fluid flow system driven by thermal convection, and controlled by these fault systems, could have delivered enough volume of dolomitization fluid and at the required temperature to account for the volume of dolostone in the Benicàssim half graben. These studies interpreted that the dolomitization fluid was composed of evolved seawater that interacted with underlying sedimentary cover and basement metamorphic rocks. Therefore, seawater drawdown and thermal convection would have not occurred at the same time. The large volume and high

reactivity of warm fluids invading the rock pores next to fault zones, and especially at their intersection, resulted in the formation of massive dolostone patches without a significant facies control. Dolostone pipes are an especial case of massive replacement around faults, since they appear rooted in the largest stratabound dolostone bodies. Their geometry and arrangement reveal that they formed when warm fluids that were focused along specific beds reached a fault and flowed upwards. Such type of structures were also described in detail by Sharp *et al*. (2010) in the Zagros Mountains.

A large volume of massive dolostone that passes laterally to a series of large-scale stratabound dolostone geobodies is associated with the Campello Fault. This huge volume of high-temperature dolostone, which forms a continuum from the fault in the north to a distance of 7 km to the south suggests that the Campello Fault was the master feeding fault (i.e. main entry point) for Mg-rich dolomitization fluids in the Benicàssim area. This interpretation is also supported by the fact that this fault also acted as the main conduit for the delivery of mineralizing fluids forming MVT in its vicinity, and also by the presence of more radiogenic burial carbonate cements occurring in the fault surroundings (Gomez-Rivas *et al*., 2014; Martín-Martín *et al*., 2015).

The role and importance of the master feeding faults on the distribution of dolostones have extensively been reported in studies of fault-controlled dolomitization (see Davies and Smith, 2006; Wilson *et al.*, 2007; Lopez-Horgue *et al*., 2010; Hollis *et al.*, 2017). In this study, the lateral dolomitization extension along the hanging wall of the master feeding fault (Campello) ranges from 790 to 1600 m for massive dolostone patches and is at least 7000 m long for stratabound dolostones (Fig. 14).

Faults that acted as barriers for dolomitization fluids can also be identified because they coincide with the termination of dolostone bodies. A series of structures ranging from outcrop fractures to large-scale faults bounding metre-thick limestone stringers or hundreds of metre-thick dolostone clusters are clearly recognized (Figs 1, 9, 10 and 11). Fault C is one of the typical examples of a low-offset (with a displacement on the order of a few metres) and large-scale (with a length of at least 2.4 km) fault that acted as a barrier for dolomitization fluids. These structures were probably not cemented when dolomitization took place, since only two pre-dolomitization marine cementation phases are found prior to replacement (Martín-Martín *et al*., 2015). Therefore, these structures caused the diversion of the dolomitization fluids either due to the presence of fault gouge or simply because they acted as planes of discontinuity for fluid flow. Similar cases of faults acting as dolomitization stoppers are rarely reported in case studies (e.g. Rustichelli *et al*., 2017), despite the fact that faults can act as barriers for fluids (Knipe *et al.*, 1998; Bense and Person, 2006; Pei *et al*., 2015). The presence of faults with similar orientation, dimensions and probably age, but that present opposite transport behaviour (i.e. acting as either conduits or barriers for dolomitizing fluids), illustrates how challenging is to predict fault permeability in the subsurface.

Finally, another structural control at the outcrop and micro scale are bedding-parallel stylolites. These structures, which pre-date replacement (Martín-Martín *et al*., 2017), acted as stoppers of the dolomitization reaction at the outcrop scale (Fig. 9H), limiting reactive flow and replacement to one of their sides. The impact of stylolites on dolomitization is discussed in more detail in Gomez-Rivas *et al*. (2015) and Martín-Martín *et al*. (2017).

Depositional controls on replacement

Dolostones in the Benicàssim area only occur in the Benassal Formation and are vertically restricted to a zone below the base of the Escucha Formation. This dolomitization zone ranges from *ca* 400 to 650 m in thickness (Fig. 12), even though the Benassal Formation is >1600 m thick. The preferred dolomitization of the uppermost part of the Benassal Formation has been interpreted to be related to the presence of a regional unconformity, which corresponds to the top of Sequence III, and the overlying of the Escucha Formation, which likely acted as a top seal for dolomitization fluids (Gomez-Rivas *et al*., 2014; Martín-Martín *et al*., 2015). Despite the similar characteristics (composition, texture, facies, etc.) of limestones of the whole Lower Cretaceous succession, the diagenetic fluids only replaced the upper part of the Benassal Formation sediments below the regional unconformity (Figs 1 and 2).

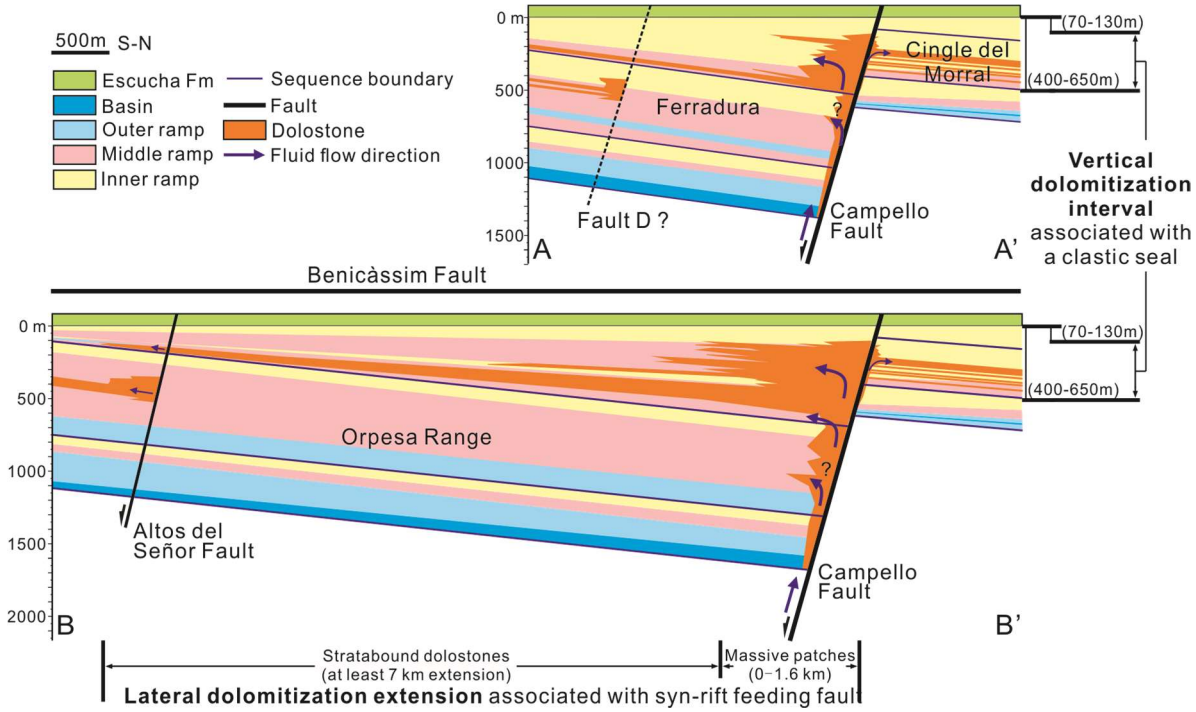

Fig. 14. Sketches of the half-graben structure showing major depositional environments (inner, middle and outer ramp) and the distribution of dolostones across the study area. Dolostones indicated with a question mark in sequence II are inferred due to lack of exposure. See Fig. 1 for section location.

There is also a 70 to 130 m thick limestone zone just below the regional unconformity at the base of the Escucha Formation which is not affected by dolomitization (Fig. 12). This configuration is very different from the frequently reported shale seals in fault-controlled dolomitization systems, where limestones just below the unconformity and sealing shale unit normally appear extensively dolomitized (see reviews by Davies and Smith, 2006 and many other case studies like Azmy and Conliffe, 2010; Saller and Dickson, 2011; Freiburg *et al*., 2012; Slater and Smith, 2012; Hendry *et al*., 2015). The presence of a non-dolomitized zone below an unconformity and clastic seal, is probably related to the composition and original porosity and permeability of such zone. In the study area, the uppermost sediments of the Benassal Formation were affected by subaerial exposure during the transition from a shallow-marine carbonate platform (Benassal Formation) to a tidal flat dominated by clastic sedimentation (base of the Escucha

Formation; Querol *et al*., 1992; Villanueva-Amadoz *et al*., 2010). This scenario is different from that described in the aforementioned carbonate systems that are overlain by shales associated with transgression and drowning which did not experience subaerial exposure and/or meteoric water cementation. Subaerial exposure in carbonates is commonly associated with significant porosity creation (karst) that may facilitate subsequent dolomitization (e.g. Sharp *et al*., 2010; Poros *et al*., 2012; Swennen *et al.*, 2012). However, they have also been reported to result in the formation of seals for dolomitizing fluids (e.g. Lavoie and Chi, 2006), likely similar to the situation in this study. In this case, a vertical dolomitization interval associated with a top seal in the Benassal Formation can be defined by subtracting the non-dolomitized zone (70 to 130 m beneath the base of the Escucha Formation) from the preferred circulation zone of dolomitization fluids (400 to 650 m beneath it; Fig. 12). What sediments are replaced within this interval depends on other factors, such as structures (see above), and facies distributions, components, texture and pre-dolomitization diagenesis (which are discussed below).

The stratigraphic framework of the Benicàssim area is mainly controlled by the activity of the two large-scale syn-rift faults (the Campello and Benicàssim faults). Therefore, these structures determined the thickness of the succession in each part of the basin and thus which parts of the Benassal Formation were located within the vertical dolomitization interval at each location. Consequently, these syn-rift faults strongly influenced the potential distribution of dolostones in the sequence stratigraphic framework (Fig. 12). The Benassal Formation is very thick in the north of the Orpesa Range (i.e. at the half graben depocentre), with the vertical dolomitization interval only affecting T-R sequence III (Fig. 5 and 12). In contrast, the Benassal Formation is relatively thinner in both the southern side of the Orpesa Range and in the Ferradura fault block, where the vertical dolomitization interval covers sediments of sequence III and the upper part of sequence II (Fig. 12). Finally, the Benassal Formation is much thinner in the Cingle del Morral fault block (Fig. 7 and 12).

The majority of dolomitized sediments in the study area were deposited in inner to middle ramp settings (Fig. 14). This observation is supported by the following facts: (i) muddy facies were deposited in outer ramp to basinal settings at the bottom of the Benassal Formation, while grainy facies were deposited in the inner ramp towards the top of the Benassal Formation, and are generally not replaced with dolomite; (ii) dolostones (both massive patches and stratabound dolostones) are most abundant in the eastern side of the study area, where middle ramp facies are prevalent; (iii) dolostones tend to replace the regressive sediments of T-R sequences when the sequence is mostly associated with an outer to middle ramp settings (such as in cases of T-R sequence II); and (iv) dolostones preferentially replace sediments around the maximum flooding zone of a T-R sequence when they represent middle to inner ramp settings (such as in case of T-R sequence III). Non-replaced limestones between or within dolostone bodies are formed by either muddy facies (e.g., spicule wackestones) with suture and sharp peak and wave-like stylolites (*sensu* Koehn *et al*., 2016) or grainy facies that are highly-cemented including pre-dolomitization marine cements (Fig. 9K and L; Martín-Martín *et al*., 2017). Both rock types were likely either impermeable to dolomitization fluids or their components were less reactive and were consequently not replaced. Reactive transport simulations indicate that a permeability contrast of at least two orders of magnitude between adjacent beds was required in order to cause preferential dolomitization of specific beds (Corbella *et al*., 2014). Additionally, Martín-Martín *et al*. (2015) revealed that replacement of calcite with dolomite started in the matrix and then affected other components. This is probably

due to the high reactive surface area of micrite. Therefore, relatively grainy (i.e. initially permeable) facies containing some micrite (e.g. wackestones and packstones) have a stronger potential for dolomitization.

The depositional setting and distribution of lithofacies are key controls on the extent of dolomitized geobodies, and normally determine the units that can be preferentially dolomitized (e.g. Barale *et al*., 2012; Hips *et al*., 2016). Previous studies indicate that fault-controlled dolomite can replace sediments deposited in a variety of environments, from relatively shallow-water settings rich in grains (e.g. Barale *et al*., 2012; Hendry *et al*., 2015) to basinal environments dominated by relatively muddy facies (e.g. Smith, 2006; Hips *et al*., 2016). However, the preferred dolomitization of wackestones to packstones seems very common in cases of fault-controlled replacement (e.g. Wilson *et al*., 2007; Beavington-Penney *et al*., 2008; Martín-Martín *et al*., 2015). This is also the case here, where the combination of initial permeability of these sediment textures together with the presence of a certain volume of micrite (with high reactive surface area) favour their replacement.

CONCLUSIONS

The results of this study reveal a series of controls on the geometry and distribution of high-temperature dolostone geobodies in extensional settings, based on the systematic study of the Benicàssim outcrop analogue. Main conclusions from this study are:

1 The strong synsedimentary activity of the west-east trending Campello Fault during the deposition of the Benassal Formation controlled the development of a half-graben basin and determined the depositional framework in the study area. As a result, the Benassal Formation is much thinner and presents shallower facies in the footwall block of the Campello Fault compared with its hanging wall.

2 The sedimentary analysis of the Benassal Formation throughout the study area reflects a depositional system with the proximal area in the west and south, and the basin depocentre towards the north-east. The carbonate succession represents a general sedimentary evolution from basinal to inner-platform depositional settings dominated by shallow-marine environments. It is characterized by the lack of deposists representing platform barriers or steps, and the scarce influx of terrigenous sediments.

3 Two end-member dolostone geometries (fault-controlled massive patches, including dolostone pipes and stratabound) have been recognized in the study area. They show a clear spatial association between the two end-members, since massive patches laterally extend to stratabound bodies. Moreover, dolostone pipes are rooted in the thickest stratabound dolostones and follow the fault plane upwards.

4 The distribution of dolostones is controlled (in order of importance) by the master feeding faults (i.e. entry points for warm dolomitization fluids), the sequence stratigraphic framework and the lithofacies. Specifically: (i) the hanging wall of the Campello and Benicàssim faults (corresponding to the basin depocentre) which was the preferred place for dolomitization, and is massive next to the faults; (ii) a clastic unit (Escucha Formation) above a regional unconformity, which corresponds to the top of the uppermost stratigraphic sequence, which acted as a seal for reactive fluids and constrained the vertical interval in which sediments could be replaced; (iii) the

thickness of transgressive and regressive sequences which determined what sediments were affected by replacement in each fault block; and (iv) deposition of the vast majority of dolomitized sediments in middle-ramp settings dominated by wackestones and packstones.

ACKNOWLEDGEMENTS

This research was funded by the University of Aberdeen, the China Scholarship Council (CSC), the AAPG (American Association of Petroleum Geologists) Foundation, and the British Sedimentological Research Group (BSRG). Additional funding was provided by the Grup Consolidat de Recerca "Geologia Sedimentària" (2017SGR-824) and DGICYT Spanish Projects CGL2015-69805-P and CGL2015-66335-C2-1-R. EGR acknowledges funding by the AGAUR (Agència de Gestió d'Ajuts Universitaris i de Recerca) of the Generalitat de Catalunya ("Beatriu de Pinós" fellowship (2016 BP 00208) and the Spanish Ministry of Science, Innovation and Universities ("Ramón y Cajal" fellowship RYC2018-026335-I). Thanks to Joan Guanyabens for his assistance during one of the field campaigns, and to Magda Chmielewska for her assistance building Lidar virtual outcrop models. We are grateful to Enric Pascual-Cebrian, Felix Schlagintweit and Telm Bover-Arnal for their suggestions on carbonate facies. We thank the reviewers Cathy Hollis and Fadi Nader and editors Hairuo Qing, Christian Betzler and Peir Pufahl for their valuable suggestions to improve this article.

REFERENCES

Allan, J.R. and **Wiggins, W.D.** (1993) Dolomite reservoirs: Geochemical techniques for evaluating origin and distribution. *AAPG Continuing Education Course Note Series*, **36**, 129 pp.

Antolín-Tomás, B., Liesa, C.L., Casas, A.M. and **Gil-Peña, I.** (2007) Geometry of fracturing linked to extension and basin formation in the Maestrazgo basin (Eastern Iberian Chain, Spain). *Revista de la Sociedad Geológica de España*, **20,** 351-365.

Azmy, K. and **Conliffe, J.** (2010) Dolomitization of the lower St. George Group on the Northern Peninsula in western Newfoundland: implications for lateral distribution of porosity. *Bull. Can. Petrol. Geol.*, **58,** 361-374.

Azmy, K., Lavoie, D., Knight, I. and **Chi, G.** (2008) Dolomitization of the Lower Ordovician Aguathuna Formation carbonates, Port au Port Peninsula, western Newfoundland, Canada: implications for a hydrocarbon reservoir. *Can. J. Earth Sci.*, **45,** 795-813.

Barale, L., Bertok, C., D'atri, A.N.N.A., Domini, G., Martire, L. and **Piana, F.** (2012) Cretaceous-Lower Eocene hydrothermal dolomitization in the Maritime Alps (NW Italy). *Rendiconti Online Della Società Geologica Italiana*, **20,** 7-9.

Beavington-Penney, S.J., Nadin, P., Wright, V.P., Clarke, E., McQuilken, J. and **Bailey, H.W.** (2008) Reservoir quality variation on an Eocene carbonate ramp, El Garia Formation, offshore Tunisia: Structural control of burial corrosion and dolomitisation. *Sed. Geol.*, **209,** 42-57.

Beckert, J., Vandeginste, V. and **John, C.M.** (2015) Exploring the geological features and processes that control the shape and internal fabrics of late diagenetic dolomite bodies (Lower Khuff equivalent – Central Oman Mountains). *Mar. Petrol. Geol.*, **68,**

325-340.

Bense, V.F. and **Person, M.A.** (2006) Faults as conduit–barrier systems to fluid flow in siliciclastic sedimentary aquifers. *Water Resour. Res.*, **42,** 1-18.

Bover-Arnal, T., Löser, H., Moreno-Bedmar, J.A., Salas, R. and **Strasser, A.** (2012) Corals on the slope (Aptian, Maestrat Basin, Spain). *Cretaceous Res.*, **37,** 43-64.

Bover-Arnal, T., Moreno-Bedmar, J.A., Frijia, G., Pascual-Cebrian, E. and **Salas, R.,** (2016) Chronostratigraphy of the Barremian-Early Albian of the Maestrat Basin (E Iberian Peninsula): integrating strontium-isotope stratigraphy and ammonoid biostratigraphy. *Newsletters on Stratigraphy*, **49/1,** 41-68.

Bover-Arnal, T., Salas, R., Guimerà, J., and **Moreno-Bedmar, J.A.,** (2014) Depp incision in an Aptian carbonate succession indicates major sea-level rise in the Cretaceous. *Sedimentology*, **61,** 1558-1593.

Bover-Arnal, T., Salas, R., Moreno-Bedmar, J.A. and **Bitzer, K.** (2009) Sequence stratigraphy and architecture of a late Early–Middle Aptian carbonate platform succession from the western Maestrat Basin (Iberian Chain, Spain). *Sed. Geol.*, **219,** 280-301.

Buckley, S.J., Enge, H.D., Carlsson, C. and **Howell, J.A.** (2010) Terrestrial laser scanning for use in virtual outcrop geology. *The Photogrammetric Record*, **25,** 225-239.

Buckley, S.J., Howell, J., Enge, H. and **Kurz, T.** (2008) Terrestrial laser scanning in geology: data acquisition, processing and accuracy considerations. *J. Geol. Soc. London*, **165,** 625-638.

Buckley, S.J., Kurz, T.H., Howell, J.A. and **Schneider, D.** (2013) Terrestrial lidar and hyperspectral data fusion products for geological outcrop analysis. *Comput. Geosci.*, **54,** 249-258.

Catuneanu, O., Abreu, V., Bhattacharya, J.P., Blum, M.D., Dalrymple, R.W., Eriksson, P.G., Fielding, C.R., Fisher, W.L., Galloway, W.E., Gibling, M.R., Giles, K.A., Holbrook, J.M., Jordan, R., Kendall, C.G.St.C., Macurda, B., Martinsen, O.J., Miall, A.D., Neal, J.E., Nummedal, D., Pomar, L., Posamentier, H.W., Pratt, B.R., Sarg, J.F., Shanley, K.W., Steel, R.J., Strasser, A., Tucker, M.E. and **Winker, C.** (2009). Towards the standardization of sequence stratigraphy. Earth-Science Reviews **92**, 1-33.

Corbella, M., Gomez-Rivas, E., Martín-Martín, J.D., Stafford, S.L., Teixell, A., Griera, A., Travé, A., Cardellach, E. and **Salas, R.** (2014) Insights to controls on dolomitization by means of reactive transport models applied to the Benicàssim case study (Maestrat Basin, eastern Spain). *Petroleum Geoscience*, **20,** 41-54.

Davies, G.R. and **Smith Jr, L.B.** (2006) Structurally controlled hydrothermal dolomite reservoir facies: An overview. *AAPG Bull.*, **90,** 1641-1690.

Dewit, J., Foubert, A., El Desouky, H.A., Muchez, P., Hunt, D., Vanhaecke, F. and **Swennen, R.** (2014) Characteristics, genesis and parameters controlling the development of a large stratabound HTD body at Matienzo (Ramales Platform, Basque-Cantabrian Basin, northern Spain). *Mar. Petrol. Geol.*, **55,** 6-25.

Dewit, J., Huysmans, M., Muchez, P., Hunt, D.W., Thurmond, J.B., Verges, J., Saura, E., Fernandez, N., Romaire, I., Esestime, P. and **Swennen, R.** (2012) Reservoir

characteristics of fault-controlled hydrothermal dolomite bodies: Ramales Platform case study. In: *Advances in Carbonate Exploration and Reservoir Analysis* (Eds J. Garland, J.E. Neilson, S.E. Laubach and K.J. Whidden), *Geol. Soc. London Spec. Publ.*, **370,** 83-109.

Diehl, S.F., Hofstra, A.H., Koenig, A.E., Emsbo, P., Christiansen, W. and **Johnson, C.** (2010) Hydrothermal Zebra Dolomite in the Great Basin, Nevada-Attributes and Relation to Paleozoic Stratigraphy, Tectonics, and Ore Deposits. *Geosphere*, **6,** 663-690.

Dunham, R.J. (1962) Classification of carbonate rocks according to depositional textures. In: *Classification of Carbonate Rocks: A Symposium* (Ed. W.E. Ham), *AAPG Mem*., **1,** 108-121.

Embry III, A.F. and **Klovan, J.E.** (1971) A late Devonian reef tract on northeastern Banks Island, NWT. *Bull. Can. Petrol. Geol.*, **19,** 730-781.

Freiburg, J.T., Fouke, B.W. and **Lasemi, Z.** (2012) *New Insights on Upper Mississippi Valley Mineralization based on Solution Cavities in the Ordovician Galena Group at the Conco Mine, North Aurora, Illinois, USA*. Illinois State Geological Survey, UAS, Circular 581, 45 pp.

Garcia, R., Moreno-Bedmar, J.A., Bover-Arnal, T., Company, M., Salas, R., Latil, J.L., Martín-Martín, J.D., Gomez-Rivas, E., Bulot, L.G., Delanoy, G., Martínez, R. and **Grauges, A.** (2014) *Lower Cretaceous (Hauterivian-Albian) ammonite biostratigraphy in the Maestrat Basin (E Spain)*. Journal of Iberian Geology, 40(1), 99-112.

Gasparrini, M., López-Cilla, I., Blázquez-Fernández, S., Rosales, I., Lerat, O., Martín-Chivelet, J. and **Doligez, B.** (2017) A multidisciplinary modeling approach to asses facies-dolomitization-porosity interdependence in a Lower Cretaceous platform (northern Spain). In: *Characterization and modeling of carbonate reservoirs* (Eds A.J. MacNeil, J. Lonnee, and R.Wood), *SEPM Spec. Publ.*, **109,** DOI: http://dx.doi.org/10.2110/sepmsp.109.07.

Gomez-Rivas, E., Corbella, M., Martín-Martín, J.D., Stafford, S.L., Teixell, A., Bons, P.D., Griera, A. and **Cardellach, E.** (2014) Reactivity of dolomitizing fluids and Mg source evaluation of fault-controlled dolomitization at the Benicàssim outcrop analogue (Maestrat basin, E Spain). *Mar. Petrol. Geol.*, **55,** 26-42.

Gomez-Rivas, E., Martín-Martín, J.D., Bons, P.D. and **Koehn, D.** (2015) Can stylolite networks control the geometry of hydrothermal alterations? *Geotectonic Research*, **97**, 34-36.

Gomez-Rivas, E., Stafford, S., Lee, A.G.K., Corbella, M., Martín-Martín, J.D. and **Teixell, A.** (2010) Flow patterns of dolomitizing solutions in a buried carbonate ramp–the Benicàssim case study (Maestrat Basin, NE Spain). In: *72nd EAGE Conference and Exhibition incorporating SPE EUROPEC 2010*, **4,** 2831–2835.

Grandia, F., Asmerom, Y., Getty, S., Cardellach, E. and **Canals, A.** (2000) U–Pb dating of MVT ore-stage calcite: implications for fluid flow in a Mesozoic extensional basin from Iberian Peninsula. *Journal of Geochemical Exploration*, **69,** 377-380.

Guimerà, J., Mas, R. and **Alonso, Á.** (2004) Intraplate deformation in the NW Iberian Chain: Mesozoic extension and Tertiary contractional inversion. *Journal of the Geological Society*, **161,** 291-303.

Hardie, L.A. (1987) Dolomitization: A critical view of some current views: perspectives. *J. Sed. Res.*, **57,** 166-183.

Hendry, J.P., Gregg, J.M., Shelton, K.L., Somerville, I.D. and **Crowley, S.F.** (2015) Origin, characteristics and distribution of fault‐related and fracture‐related dolomitization: Insights from Mississippian carbonates, Isle of Man. *Sedimentology*, **62,** 717-752.

Hips, K., Haas, J. and **Győri, O.** (2016) Hydrothermal dolomitization of basinal deposits controlled by a synsedimentary fault system in Triassic extensional setting, Hungary. *International Journal of Earth Sciences*, **105,** 1215-1231.

Hollis, C., Bastesen, E., Boyce, A., Corlett, H., Gawthorpe, R., Hirani, J., Rotevatn, A. and **Whitaker, F.F.** (2017) Fault-controlled dolomitization in a rift basin. *Geology*, **45,** 219-222.

Howell, J.A., Martinius, A.W. and **Good, T.R.** (2014) The application of outcrop analogues in geological modelling: A review, present status and future outlook. *Geol. Soc. London Spec. Publ.*, **387,** 1-25.

Humphrey, E., Gomez-Rivas, E., Neilson, J., Martín-Martín, J.D., Healy, D., Yao S. and Bons, P.D. (2020) Quantitative analysis of stylolite networks in different platform carbonate facies. *Marine and Petroleum Geology*, in press.

Jacquemyn, C., Huysmans, M., Hunt, D., Casini, G. and **Swennen, R.** (2015) Multi-scale three-dimensional distribution of fracture-and igneous intrusion-controlled hydrothermal dolomite from digital outcrop model, Latemar platform, Dolomites, northern ItalyThree-dimensional Dolomite Distribution. *AAPG Bull.*, **99,** 957-984.

James, N.P. and **Jones, B.** (2015) *Origin of Carbonate Sedimentary Rocks*. John Wiley & Sons Ltd., New Jersey, 464 pp.

Knipe, R.J., Jones, G. and **Fisher, Q.J.** (1998) Faulting, fault sealing and fluid flow in hydrocarbon reservoirs: an introduction. *Geol. Soc. London Spec. Publ.*, **147,** vii-xxi.

Koehn, D., Pataki-Rood, M., Beaudoin, N., Chung, P., Bons, P.D. and **Gomez-Rivas, E.** (2016). A new stylolite classification scheme to estimate compaction and local permeability variations. *Sedimentary Geology*, 346, 60-71.

Lapponi, F., Casini, G., Sharp, I., Blendinger, W., Fernández, N. and **Hunt, D.** (2011) From outcrop to 3D modelling: a case study of a dolomitized carbonate reservoir, Zagros Mountains, Iran. *Petroleum Geoscience*, **17,** 283-307.

Lavoie, D. and **Chi, G.** (2006) Hydrothermal dolomitization in the Lower Silurian La Vieille Formation in northern New Brunswick: geological context and significance for hydrocarbon exploration. *Bull. Can. Petrol. Geol.*, **54,** 380-395.

Lavoie, D., Chi, G., Urbatsch, M. and **Davis, W.J.** (2010) Massive dolomitization of a pinnacle reef in the Lower Devonian West Point Formation (Gaspé Peninsula, Quebec): An extreme case of hydrothermal dolomitization through fault-focused circulation of magmatic fluids. *AAPG Bull.*, **94,** 513-531.

López-Horgue, M., Iriarte, E., Schröder, S., Fernández-Mendiola, P.A., Caline, B., Corneyllie, H., Frémont, J., Sudrie, M. and **Zerti, S.** (2010) Structurally controlled hydrothermal dolomites in Albian carbonates of the Asón valley, Basque Cantabrian Basin, Northern Spain. *Mar. Petrol. Geol.*, **27,** 1069-1092.

Machel, H.G. (2004) Concepts and models of dolomitization: a critical reappraisal. *Geol.*

Soc. London Spec. Publ., **235,** 7-63.

Mansurbeg, H., Morad, D., Othmana, R., Morad, S., Ceriani, A., Al-Aasm, I., Kolo, K., Spirov, P., Proust, J.N., Preat, A. and Koyi, H. (2016). Hydrothermaldolomitization of the Bekhme formation (Upper Cretaceous), Zagros Basin, Kurdistan Region of Iraq: Record ofoil migration and degradation. *Sed. Geol.*, **341,** 147-162.

Martín-Martín, J.D., Gomez-Rivas, E., Bover-Arnal, T., Travé, A., Salas, R., Moreno-Bedmar, J.A., Tomás, S., Corbella, M., Teixell, A., Vergés, J. and **Stafford, S.L.** (2013) The Upper Aptian to Lower Albian syn-rift carbonate succession of the southern Maestrat Basin (Spain): Facies architecture and fault-controlled stratabound dolostones. *Cretaceous Res.*, **41,** 217-236.

Martín-Martín, J.D., Gomez-Rivas, E., Gómez-Gras, D., Travé, A., Ameneiro, R., Koehn, D. and **Bons, P.D.** (2017) Activation of stylolites as conduits for overpressured fluid flow in dolomitized platform carbonates. *Geol. Soc. London Spec. Publ.*, **459,** 157-176.

Martín-Martín, J.D., Travé, A., Gomez-Rivas, E., Salas, R., Sizun, J.P., Vergés, J., Corbella, M., Stafford, S.L. and **Alfonso, P.** (2015) Fault-controlled and stratabound dolostones in the Late Aptian–earliest Albian Benassal Formation (Maestrat Basin, E Spain): petrology and geochemistry constrains. *Mar. Petrol. Geol.*, **65,** 83-102.

Morrow, D.W. (2014) Zebra and boxwork fabrics in hydrothermal dolomites of northern Canada: Indicators for dilational fracturing, dissolution or in situ replacement? *Sedimentology*, **61,** 915-951.

Nadal, J. (2001) *Estudi de la dolomitització del Juràssic superior-Cretaci inferior de la Cadena Ibérica oriental y la Cadena Costanera Catalana: relació amb la segona etapa de rift mesozoica*. PhD thesis, Universitat de Barcelona, Barcelona, 416 pp.

Pei, Y., Paton, D.A., Knipe, R.J. and **Wu, K.** (2015) A review of fault sealing behaviour and its evaluation in siliciclastic rocks. *Earth-Sci. Rev.*, **150,** 121-138.

Poros, Z., Mindszenty, A., Molnár, F., Pironon, J., Győri, O., Ronchi, P. and **Szekeres, Z.** (2012) Imprints of hydrocarbon-bearing basinal fluids on a karst system: mineralogical and fluid inclusion studies from the Buda Hills, Hungary. *International Journal of Earth Sciences*, **101,** 429-452.

Qing, H. and **Mountjoy**, E. (1992) Large-scale fluid flow in the Middle Devonian Presqu'ile barrier, Western Canada Sedimentary Basin. *Geology*, **20**, 903-906.

Qing, H. and **Mountjoy**, E. (1994) Formation of coarsely crystalline, hydrothermal dolomite reservoirs in the Presqu'ile barrier, Western Canada Sedimentary Basin. *American Association of Petroleum Geologists Bulletin*, **78**, 55-77.

Querol, X., Salas, R., Pardo, G. and **Ardevol, L.** (1992) Albian coal-bearing deposits of the Iberian Range in northeastern Spain. *Controls on the distribution and quality of Cretaceous coals*, **267**, 193-208.

Roca, E. and **Guimerà, J.** (1992) The Neogene structure of the eastern Iberian margin: structural constraints on the crustal evolution of the Valencia trough (western Mediterranean). *Tectonophysics*, **203,** 203-218.

Roehl, P.O. and **Choquette, P.W.** (2012) *Carbonate petroleum reservoirs*. Springer-Verlag, New York, 622 pp.

Ronchi, P., Masetti, D., Tassan, S. and **Camocino, D.** (2012) Hydrothermal dolomitization in platform and basin carbonate successions during thrusting: A hydrocarbon reservoir analogue (Mesozoic of Venetian Southern Alps, Italy). *Mar. Petrol. Geol.*, **29,** 68-89.

Rustichelli, A., Iannace, A., Tondi, E., Celma, C.D., Cilona, A., Giorgioni, M., Parente, M., Girundo, M. and **Invernizzi, C.** (2017) Fault-controlled dolomite bodies as palaeotectonic indicators and geofluid reservoirs: New insights from Gargano Promontory outcrops. *Sedimentology*, **64,** 1871-1900.

Salas, R. and **Casas, A.** (1993) Mesozoic extensional tectonics, stratigraphy and crustal evolution during the Alpine cycle of the eastern Iberian basin. *Tectonophysics*, **228,** 33-55.

Salas, R., Guimerà, J., Mas, R., Martín-Closas, C., Meléndez, A. and **Alonso, A.** (2001) Evolution of the Mesozoic central Iberian Rift System and its Cainozoic inversion (Iberian chain). *Peri-Tethys Memoir*, **6,** 145-185.

Saller, A.H. and **Dickson, J.A.T.D.** (2011) Partial dolomitization of a Pennsylvanian limestone buildup by hydrothermal fluids and its effect on reservoir quality and performance. *AAPG Bull.*, **95,** 1745-1762.

Shah, M.M., Nader, F.H., Dewit, J., Swennen, R. and **Garcia, D.** (2010) Fault-related hydrothermal dolomites in Cretaceous carbonates (Cantabria, northern Spain): Results of petrographic, geochemical and petrophysical studies. *Bulletin de la Société Géologique de France*, **181,** 391-407.

Sharp, I., Gillespie, P., Morsalnezhad, D., Taberner, C., Karpuz, R., Vergés, J., Horbury, A., Pickard, N., Garland, J. and **Hunt, D.** (2010) Stratigraphic architecture and fracture-controlled dolomitization of the Cretaceous Khami and Bangestan groups: an outcrop case study, Zagros Mountains, Iran. *Geol. Soc. London Spec. Publ.*, **329,** 343-396.

Sibley, D.F. and **Gregg, J.M.** (1987) Classification of dolomite rock textures. *J. Sed. Res.*, **57,** 967-975.

Slater, B.E. and **Smith Jr, L.B.** (2012) Outcrop analog for Trenton–Black River hydrothermal dolomite reservoirs, Mohawk Valley, New York. *AAPG Bull.*, **96,** 1369-1388.

Smith Jr, L.B. (2006) Origin and reservoir characteristics of Upper Ordovician Trenton–Black River hydrothermal dolomite reservoirs in New York. *AAPG Bull.*, **90,** 1691-1718.

Strasser, A., Pittet, B., Hillgärtner, H. and **Pasquier, J. B.** (1999) Depositional sequences in shallow carbonate-dominated sedimentary systems: concepts for a high-resolution analysis. *Sedimentary Geology*, **128**, 201-221.

Swennen, R., Dewit, J., Fierens, E., Muchez, P., Shah, M., Nader, F. and **Hunt, D.** (2012) Multiple dolomitization events along the Pozalagua Fault (Pozalagua Quarry, Basque–Cantabrian Basin, Northern Spain). *Sedimentology*, **59,** 1345-1374.

Thompson, D.L., Stilwell, J.D. and **Hall, M.** (2015) Lacustrine carbonate reservoirs from Early Cretaceous rift lakes of Western Gondwana: Pre-salt coquinas of Brazil and West Africa. *Gondwana Research*, **28,** 26-51.

Tomás, S., Löser, H. and **Salas, R.** (2008) Low-light and nutrient-rich coral assemblages

in an Upper Aptian carbonate platform of the southern Maestrat Basin (Iberian Chain, eastern Spain). *Cretaceous Res.*, **29,** 509-534.

Tucker, M.E. (2009) *Sedimentary petrology: an introduction to the origin of sedimentary rocks*. John Wiley & Sons, 272 pp.

Vandeginste, V., John, C.M., van de Flierdt, T. and **Cosgrove, J.W.** (2013) Linking process, dimension, texture, and geochemistry in dolomite geobodies: A case study from Wadi Mistal (northern Oman) Linking Process, Dimension, Texture, and Geochemistry in Dolomite Geobodies. *AAPG Bull.*, **97,** 1181-1207.

Villanueva-Amadoz, U., Pons, D., Diez, J.B., Ferrer, J. and **Sender, L.M.** (2010) Angiosperm pollen grains of San Just site (Escucha Formation) from the Albian of the Iberian Range (north-eastern Spain). *Rev. Palaeobot. Palynol.*, **162,** 362-381.

Warren, J. (2000) Dolomite: occurrence, evolution and economically important associations. *Earth-Sci. Rev.*, **52,** 1-81.

Whitaker, F.F., Smart, P.L. and **Jones, G.D.** (2004) Dolomitization: from conceptual to numerical models. *Geol. Soc. London Spec. Publ.*, **235,** 99-139.

Wilson, M.E., Evans, M.J., Oxtoby, N.H., Nas, D.S., Donnelly, T. and **Thirlwall, M.** (2007) Reservoir quality, textural evolution, and origin of fault-associated dolomites. *AAPG Bull.*, **91,** 1247-1272.